Alma Mater Studiorum · Università di Bologna

Scuola di Scienze
Dipartimento di Fisica e Astronomia
Corso di Laurea in Fisica

Analysis of the XX century trends in the global Sea Surface Temperature

Relatore:
Prof. Antonio Navarra

Presentata da:
Adele Marascio

Anno Accademico 2022/2023

Sommario

La Temperatura della Superficie del Mare (SST) rappresenta un parametro fondamentale per valutare i cambiamenti meteorologici e climatici su scale temporali da interannuali a decennali, poiché la sua variabilità riflette la maggior parte del sistema atmosferico-oceanico accoppiato e influenza il clima globale. In questa tesi viene analizzato il set di dati Hadley Sea Ice and Sea Surface Temperature (HadISST) [7] per investigare i trend lineari delle SST nei cinque periodi trentennali dal 1870 al 2020 e vengono evidenziate le variabilità stagionali e interannuali negli Oceani Pacifico, Indiano e Atlantico. Il risultato è un aumento della media globale della SST, ma sono visibili anche regioni di raffreddamento e riscaldamento localizzate le cui cause vengono spiegate nel contesto della variabilità naturale e dell'aumento dei gas serra. Inoltre, una simulazione storica delle SST, Euro-Mediterranean Centre on Climate Change coupled Climate Model Version 2 (CMCC-CM2) [3], viene utilizzata per calcolare i trend nel periodo 1950-2014, poi confrontati con i dati osservativi di HadISST e con simulazioni provenienti dal Coupled Model Intercomparison Project 6 (CMIP6) [5] e dal Large Ensemble Project (LENS) [6]. Si osserva che, come per le medie di CMIP6 e LENS, la simulazione CMCC-CM2 rappresenta erroneamente un trend di riscaldamento in una zona del Pacifico Equatoriale in cui non si registra aumento di temperatura.

Abstract

Sea Surface Temperature (SST) represents a significant parameter for assessing weather and climate changes on interannual to decadal time scales, as its variability reflects the vast majority of the coupled atmospheric-oceanic system and affects the global climate. Within this thesis the Hadley Centre's Sea Ice and Sea Surface Temperature data set (HadISST) [7] is analysed to investigate the linear SST trends over five thirty-year periods from 1870 to 2020. Seasonal and interannual variability in the Pacific, Indian, and Atlantic Oceans is highlighted. The result is a global increase of mean SST with regions of localized cooling and warming, the causes of which are explained within internal variability or the rising of greenhouse gases. Linear trends are also performed on an historical SST simulation of the period from 1950 to 2014 from the Euro-Mediterranean Centre on Climate Change coupled Climate Model Version 2 (CMCC-CM) [3], and then compared with observational HadISST data, and simulations from the Coupled Model Intercomparison Project 6 (CMIP6) [5] and from the Large Ensemble Project (LENS) [6]. It is observed that, as in CMIP6 and LENS means, CMCC-CM2 misrepresent a zone in the Equatorial Pacific depicting sustained heating, where it is actually absent.

Contents

Introduction

The Sea Surface Temperature (SST) is the bulk temperature of the ocean, referring to the top layer, where the water interacts with the hydrosphere. SST plays a significant role in understanding the dynamics of the Earth's climate system, as it influence various phenomena, including weather patterns, ocean currents, marine ecosystems, and global climate trends. These elements interact to create dynamic temperature variations across different oceanic regions; hence SST is the basis for the interaction between the ocean and the atmosphere. As a result, SST exhibits both spatial and temporal variability, with variations occurring on daily, seasonal, and long-term time scales.

Over time, measuring SST has been accomplished using different methods, including in-situ measurements from buoys, ships, drifters and autonomous instruments, and, since the '80s, satellite-based remote sensing, as well as historical data collected over decades. Collecting observation is then followed by reconstruction of missing data and data analysis, in order to evaluate pattern of variability and effectuate prevision on the future weather and climate.

Small variations of SST are connected to the intensity and frequency of internal variability factors. The mean state of the tropical Pacific, for instance, modulates the El Niño–Southern Oscillation (ENSO)[13], the dominant mode of internannual to decadal time scale global climate variability, and the reach of the oceanic current of the Atlantic Meridional Overturning Circulation (AMOC) is said to be related to the SST gradient in the Northern Atlantic, with crippling consequences on European and North American climate [1]. Small changes in the SST gradient in the Indian and Pacific equatorial oceans drive precipitation changes in much of the extratropics.

Since SST measuring can detect upwelling events, calculating trends can serve as a valuable index for assessing the richness and vitality of marine ecosystems, threatened by the warming that is afflicting the global oceans since the beginning of the XX century. Sea surface temperature is then a fundamental physical parameter of the climate system, well suited for monitoring climate change due to the large thermal inertia of the oceans compared with that of the atmosphere and surface land [14]. When projecting the future of global climate, one of the parameter to consider is how much heat and CO_2 the ocean can absorb, and SST also reflects sea–air heat and water vapor exchange [10]. On the other hand, decadal cold state

of the Equatorial Pacific have been connected to increased ocean heat uptake and reduced global warming [18].

XX century SST trends are subject to considerable uncertainty, limiting their physical interpretation and utility as verification for climate model simulations. This uncertainty is especially evident in the tropical Pacific where the scientific community is still debating the biases which the models are subject to. According to Seager et al. [21], models are biased and can't reproduce seamlessly the equatorial Pacific SSTs trends, while according to Olonscheck et al. [13] climate models are able to capture the major patterns of variability, considering a larger picture: simulations have the purpose to reproduce trends over 20-30 years periods rather than guessing a local variable at a specific time.

So it is evident the vital role that SST trends hold in climate and environmental science, and how much it is important to reconstruct the causal relationship between oceanic and atmospheric phenomena to forecast the future of the climate system.

In this thesis, the data set analysed is the Met Office Hadley Centre's Sea Ice and Sea Surface Temperature (HadISST) [7], treating solely SSTs. The aim of this work is to evaluate global Sea Surface Temperature trends over five periods of 30 years each from 1870 to 2020, observing the rising magnitude of heating trough time, in particular the visible acceleration of the last 30 years. Trends are investigated focusing on regions of special interest for the worldwide climate and weather, introducing the main factors of seasonal to interannual variability, both natural and anthropogenic. Finally, the observed global trends from HadISST are going to be compared to the historical global trends interpolated by the CMCC Climate Model 2 [3] and to the simulated trends regarding the equatorial Pacific region from the work of Seager et al.[21] in order to find analogies and differences.

In Chapter 1 the HadISST data-set is introduced, along with an overview of how measurements are collected, manipulated and interpreted before they can constitute a complete global data-set.

Chapter 2 describes the fondant of physical oceanography, some mechanisms of interaction in the coupled ocean-atmosphere system and how they affect SSTs, highlighting the distinction between external and internal climate forcing.

Chapter 3 presents how the statistical analysis has been conducted. SST trends in the northern and equatorial Pacific, northern Atlantic and Indian Oceans are described, focusing on anomalies and exposing some factors of variability, including how greenhouse gases affects the atmosphere-ocean coupled system dynamics.

Chapter 4 summarizes how the state-of-the-art climate models process physical data to reconstruct the past and forecast the future of the climate system, including their current limits and inaccuracies. As an example, an historical simulation from the CMCC-CM2 model is performed, then compared to the HadISST data set and to CMIP6 and LENS.

Chapter 1

The HadISST Data Set

The Met Office Hadley Centre's Sea Ice and Sea Surface Temperature (HadISST) data set is a combination of monthly globally complete fields of SST and sea ice concentration on a 1°latitude-longitude grid from 1870 to 2020. It replaces the previous Global Sea Ice and Sea Surface Temperature (GISST).

The SST data are taken from the climate research institution Met Office Marine Data Bank (MDB), which from 1982 onward also includes data received through the Global Telecommunications System (GTS), the communication network that enables real-time exchange of meteorological data from weather stations, satellites and numerical weather prediction centres. Where MDB data were not available, monthly median SSTs for 1871-1995 from the Comprehensive Ocean-Atmosphere Data Set (COADS, now ICOADS) were included [7].

Data is used for a spatially complete, monthly SST analysis for 1870 to date, preserving real climate signals on different geographical scales, while minimizing random errors, sampling noise, and systematic biases.

The HadISST/GISST family is unique among available integrated SST and sea ice analyses in being globally complete while spanning well over a century, while other SST data set describe shorter periods of time, being developed for different purposes. The data set is based on a combination of in-situ observations, satellite data, and statistical methods. If missing, data are reconstructed using a two-stage reduced-space optimal interpolation procedure, followed by superposition of quality-improved gridded observations onto the reconstructions to restore local detail [7].

1.1 Empirical Orthogonal Functions

Empirical orthogonal function analysis (EOF) is a method of data reconstruction widely used in historical data set to capture the major mode of SST variability and to project them onto the available SST observation. EOFs are an abstract mathematical representation of climate data. They are used, for instance, when traditional in-situ measurements need to be blended with satellite observation.

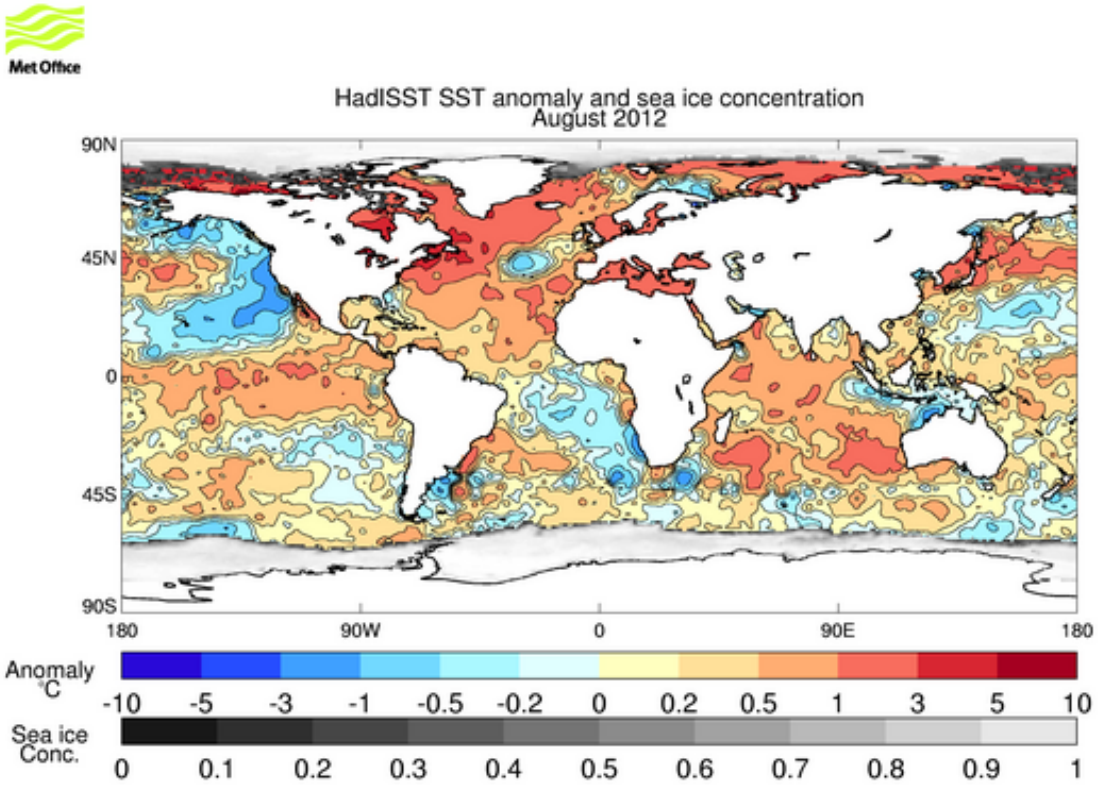

Figure 1.1: SST Anomalies and Sea Ice concentration on August 2012 from the HadISST data set. Source: Met Office.

EOF analysis is based on the assumption that the time evolution of climate processes entails relationships between time series of different atmospheric variables, both in nearby and remote locations, and its aim is to identify the most significant patterns. Analyzing the correlation between different physical variables is fundamental to interpret the climate system as a whole.

Climate observations are organized in regular spatial grid and time series, with defined and homogeneous time-spatial resolution when possible. Climate scientists classifies data, as it comes natural, in three dimensional fields, namely latitude, longitude and time. A useful representation is the data matrix $\mathbf{X}$:

$$\mathbf{X} = \begin{bmatrix} x_1(1) & x_1(2) \dots x_1(n) \\ x_2(1) & x_2(2) \dots x_2(n) \\ & \vdots \\ x_m(1) & x_m(2) \dots x_m(n) \end{bmatrix}$$

Where each row vector $\mathbf{x_i} = (x_i(1), x_i(2), ..., x_i(n))$ represents n time observation at the same location. On the other hand, the synoptic view is the visualization at the same time of m locations, and corresponds to the column vector of $\mathbf{X}$. Each

synoptic vector is, indeed, a map, and represents a vector in the n-dimensional data space, which covers all combinations of temperature, even the highly unlikely ones. Correlation between synoptic vectors can be emphasised searching for linear dependency in a time series. Because of that it is necessary to evaluate the independent mode of variation and their contribution to the total variance and this is obtained by performing Singular Value Decomposition on the covariance matrix.

1.1.1 Singular Value Decomposition

Singular Value Decomposition (SVD) is a procedure of diagonalization of squared as well as rectangular matrices. Any $m \times n$ matrix $\mathbf{A}$ can be transformed as:

$$\mathbf{A} = \mathbf{U}\mathbf{\Sigma}\mathbf{V}^* \tag{1.1}$$

Where $\mathbf{U}$ and $\mathbf{V}$ are squared orthogonal matrices of dimension m and n respectively. Their columns are called, respectively, left and right singular vectors. Matrix $\mathbf{\Sigma}$ is diagonal, and its real non-negative elements, σ_i, defined as singular values, are sorted in ascending order. It is demonstrated that left singular vectors are the eigenvectors of $\mathbf{A}\mathbf{A}^*$, while right singular vectors are eigenvectors for $\mathbf{A}^*\mathbf{A}$. The rank of the matrix is the number of non-zero singular values. So the problem of finding the number of linearly independent components can be simplified by performing SVD.

In HadISST case, the data vectors are 180×360 grids, but performing SVD reduces notably computation times and costs.

Consider the data matrix $\mathbf{X}$ with elements $x_{i,j}$, and the time series x_i with mean value $\bar{x_i}$. The covariance matrix S is a symmetric matrix with each element $s_{j,k}$:

$$s_{j,k} = \frac{1}{n-1}\sum_{i=1}^{n} k^2(x_{j,i} - \bar{x_j})(x_{k,i} - \bar{x_k}) \tag{1.2}$$

so that $s_{j,j} = s_j^2$ is the variance of the jth variable while $s_{j,k}$ is the covariance between the jth and the kth variables.

The data matrix can be transformed into having zero as mean vector by subtraction of the mean value of each row $\bar{x}$ to each element. Once $\mathbf{X}$ has been decomposed as:

$$\mathbf{X} = \mathbf{U}\mathbf{\Sigma}\mathbf{V}^{\mathbf{T}} \tag{1.3}$$

And noting that:

$$\mathbf{S} = \frac{1}{n-1}\mathbf{X}\mathbf{X}^{\mathbf{T}} \tag{1.4}$$

It is possible to see that:

$$\mathbf{S} = \mathbf{U}\mathbf{\Sigma}^{\mathbf{2}}\mathbf{U}^{\mathbf{T}} \tag{1.5}$$

So the number of independent maps in the data sets, namely the columns of $\mathbf{U}$, is the same as the eigenvectors of the covariance matrix. The vectors in the unitary matrix $\mathbf{U}$ are such that the covariance matrix in that basis is diagonal, that is each

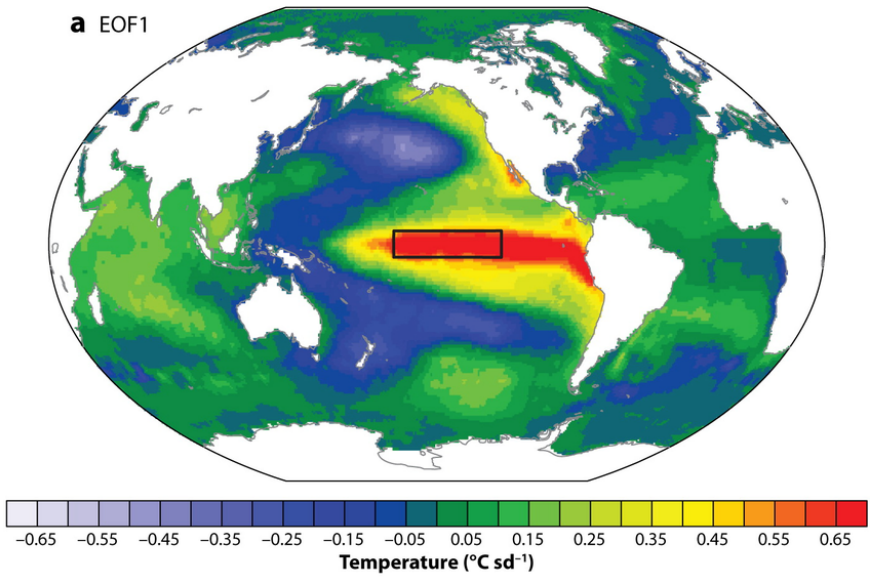

Figure 1.2: Leading empirical orthogonal function (EOF) of detrended monthly sea surface temperature (SST) anomalies over the global oceans based on the HadISST data set during 1900–2008. This mode, which accounts for 19% of the variance, depicts the El Niño-Southern Oscillation phenomenon. Source: Deser et al.[4]

vector $\mathbf{u}$, or mode of variation, is uncorrelated with the others and contributes to the total variance an amount given by the diagonal element of $\mathbf{\Sigma^2}$.

Because of the invariance property of the trace, the total variance is also given by the sum of the squared singular values σ_i^2. Dividing the latter by the trace, it is obtained the percentage contribution μ_i of each mode of variation:

$$\mu_i = \frac{\sigma_i^2}{\sum_{i=1}^{n} \sigma_i^2} \tag{1.6}$$

Once SVD has been computed it is possible to see that an entire data set can be reconstructed using only a few independent vectors. The explained variance shows which eigenvectors are actually important and which contribute to the total variance in a non significant way, usually the number of significant eigenvectors being the smallest between the time series length n and the number of spatial location m.

EOFs present themselves as spacial structures, alternating positive and negative centers required by orthogonality, whose complication grows with the decrease of significance, as a sort of higher order correction.

Since the independent mode of variation form a basis $\mathbf{u}$, data can be reconstructed by linear combination weighted by the singular values, with coefficients obtained by projecting each data vector onto each EOF:

$$\mathbf{x_k} = \sum_{i=1}^{n} \mathbf{u_i} \sigma_i \mathbf{v_i}(k) \tag{1.7}$$

A possible incoming issue in EOF analysis is the treatment of noise. Noise in a data set refers to random fluctuations or irregularities that can obscure the underlying patterns of interest; the problem is that there is no clear and absolute distinction between signal and noise, as what is noise for a measure can be signal for another one.

Compared to the dominant modes, noise is generally considered to be less systematic and less coherent. As a result, EOFs tend to focus on capturing the structured and coherent variability in the data while suppressing the less significant ones, and the determination of the latter is usually an empirical issue. This process is referred as truncating. Analysis or reconstruction is then performed only by the higher modes, and the reconstructed data set is a smoothed and simplified version of the original data. So the prominent features are highlighted and the noise is minimized.

1.2 Data Reconstruction

As mentioned above, for the most data-sparse region a certain degree of manipulation is needed before the data set can be considered complete.

The Met Office uses Reduced Space Optimal Interpolation (RSOI), a data assimilation technique based on EOFs which combines in-situ and remotely sensed SST observation. This methods uses a set of fixed EOFs, E, as defined above, describing the characteristic spatial patterns of SST anomaly variations in a generally well-observed period.

It is assumed that the same set of patterns dominated throughout the period of reconstruction, and that the magnitude of their amplitudes remained the same. The set of EOFs, E, truncated to admit real signals and exclude noise, is used to reconstruct past fields of Sea Surface Temperature, T, via a vector of time coefficients, a: $T = Ea$. The reconstruction is then fitted to the incomplete, gridded observed data, T_o, for each historical month in a least squares sense in EOF space, determining a for all EOFs used [7].

Chapter 2

Ocean and Atmosphere Interaction

The global climate system is the result of a mechanism that involves multiple parts: the hydrosphere, land surface, the cryosphere, the biosphere, and atmosphere; in particular ocean dynamics and chemical-physical properties of seawater have an outsize role.

Since SSTs are responsible for the exchange of turbulent and radiative energy, several atmospheric parameters such as wind speed, humidity, air temperature and cloudiness are deeply connected to them.

2.1 Forcings

The identification of the forcings of a given dynamical system is of course depending on the definition on the system itself. In the case of the climate system, usually they are divided in natural and anthropic, depending if they are generated by natural processes or human activities.

Climate variability is then composed of two parts: the first can be reconducted through a chain of processes to the external forcings and the second that cannot be explained by the external forcings and it is due to the intrinsic internal dynamics of the climate system, the internal variability.

The internal variability requires no external forcing to exist, but the forced response can be excited by natural or human-induced factors that can be either positive (warming) or negative (cooling). Natural climate forcings include volcanic eruptions, solar radiation variations, and changes in Earth's orbit. Human-induced forcings, primarily driven by greenhouse gas emissions, trap heat in the atmosphere and enhance the greenhouse effect, resulting in global warming. External forcing may also generate new patterns of atmospheric circulation response.

However, a both kinds of variability depend on the interaction between ocean and atmosphere, which is essentially regulated by wind driven current and termohaline

circulation. The first is due to impulse transfer from surface-tangential winds and the latter derives from change in salinity and temperature. Although their causes are different, they cannot be separated into two well-distinguished mechanism since they are deeply connected and influence each other.

2.2 Basic concepts in ocean dynamics

To maintain equilibrium, oceanic masses are distributed in layers of density that increase with depth. Except than in the higher latitude, the ocean is divided into three zones: mixed layer, pycnocline and deep layer. The pycnocline indicate a rapid variation in density, but also in temperature (thermocline) or salinity (halocline), creating two masses of unmixable waters. Wind driven current are also confined to the surface (within ∼100m of depth) because the pycnocline works as a separation layer preventing the transfer of kinetic energy and vertical mixing.

The laws of motion are Newton's equations, expressed as the Navier-Stokes equations. For a fluid element located at $\mathbf{x}$=(x,y,z) on the surface of our rotating planet, and moving at velocity $\mathbf{v}$=(v_x,v_y,v_z) relative to that surface, the equations are:

- the zonal and meridional momentum equation:

$$\frac{Dv_x}{Dt} = -\frac{1}{\rho}\frac{\delta p}{\delta x} + 2\Omega v_x \sin\phi + \frac{1}{\rho}\frac{\delta \tau_x}{\delta z} \tag{2.1}$$

$$\frac{Dv_y}{Dt} = -\frac{1}{\rho}\frac{\delta p}{\delta y} - 2\Omega v_x \sin\phi + \frac{1}{\rho}\frac{\delta \tau_y}{\delta z} \tag{2.2}$$

- the hydrostatic balance:

$$\frac{\delta p}{\delta z} = -\rho g \tag{2.3}$$

- the continuity equation:

$$\nabla \cdot \mathbf{v} = 0 \tag{2.4}$$

- the temperature equation:

$$\frac{\delta T}{\delta t} + \mathbf{v} \cdot \nabla T = Q \tag{2.5}$$

- the salinity equation:

$$\frac{\delta S}{\delta t} + \mathbf{v} \cdot \nabla S = (E - P)S(z = 0) \tag{2.6}$$

with ρ, p being seawater density and pressure, Ω the Earth angular velocity, the angle ϕ the latitude, τ the deviatoric stress, T the temperature, Q the heat input to the ocean, and $P - E$ is the freshwater input to the ocean.

2.2.1 Ekman Transport and Geostrophic Current

Because of friction, wind drags a column of water of 10-100 metres that due to the Coriolis effect, moves at a net 90° angle from the direction of the surface wind. The movement is not homogeneous in the water column: the upper thin layer rotates of 45° and it leads to the movement of the one below, this one rotating of a smaller angle, and so on, with a decreasing magnitude of velocity until it dissipates completely. In the Northern hemisphere, transport occurs clockwise from wind direction, while in the Southern hemisphere it occurs at anticlockwise direction. Exactly as the Coriolis effect, this rotation is null at the Equator. In the subtropics, the Ekman transport causes the convergence of water driven by trade winds and the rise of their level, leading to zone of high pressure.

This zones of higher pressure do not lead to lateral flux from high to low pressure regions as one might think, once again because of the Coriolis effect. At deep levels circular currents establish, which evolve along the isobars, lines of equal pressure. In this mechanism, the Coriolis force, which is radial and direct towards the centre of the bulge, is compensated by the pressure gradient force, which is also radial, but outwards directed. This equilibrium defines the geostrophic current and leads to anti-cyclonic gyre in the sub-tropics. The geostrophic current of a subtropical gyre is clockwise in NH and anti-clockwise in SH. Hence the horizontal movement of the water reflects the atmospheric circulation; in particular the geostrophic equilibrium implies the appearance of currents whenever there's a change in sea level or pressure.

2.2.2 Thermohaline Convection

Unlike surface currents, which are primarily influenced by wind patterns, thermohaline convection operates at much deeper levels and is driven by density gradients, which, in turn, depends on two main factors: temperature and salinity.

Wind driven currents move polewards, and seawater cools at high latitudes. Here it becomes denser due to lower temperatures and to ice formation, which retains a lower percentage of salts. This creates a heavier mass that has a tendency to sink, down to 2000 metres and beyond. This dense, cold water forms the basis of the deep ocean currents. As this deep water flows towards the equator, it gradually gets warmed by the sun's energy, and as a result, it rises back towards the surface. This upwelling completes the convective cycle, connecting various ocean basins and creating a continuous flow of water around the globe (Fig. 2.2). The thermohaline convection (THC), also referred as conveyor belt, is distinguished from the Meridional Overturning Circulation (MOC) which comprehends the wind transport.

2.3 The Meridional Overturning Circulation

MOC plays a crucial role in regulating the global climate as it helps transport heat and moisture between different regions of the world.

In areas where the MOC brings warm and saline-rich waters northward, the SST may be higher compared to other ocean regions. Similarly, in areas where the MOC brings cold water from the north to the south, the Sea Surface Temperature may be lower. MOC variations can display long term effects on global climate and vice versa changes in SSTs lead to significant consequence on ocean circulation.

The reach of thermohaline circulation exhibits strong decadal oscillation and may experience significant changes in response to global warming.

A study led by Semenov and Latif, performed on a 500 years long simulation on a ocean-atmosphere general circulation model, demonstrated that MOC reduces its flow considerably, of about one Sverdrup (1Sv= $10^3 m^3/s$), when the Pacific SSTs don't vary interannually [22].

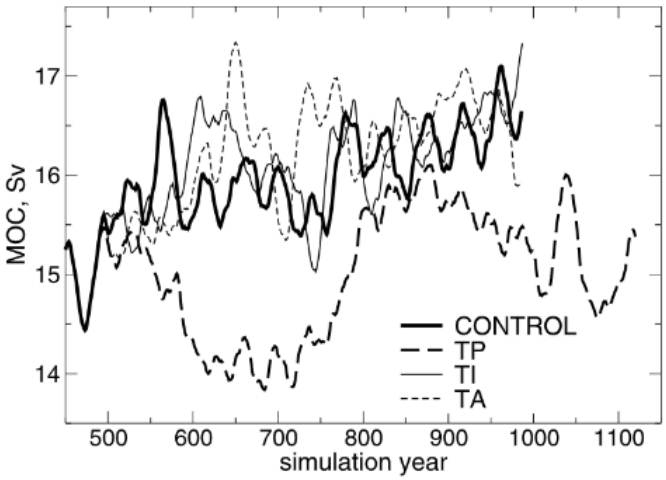

Figure 2.1: Simulations of MOCs at 20S-20N with removed interannual SSTs variability, compared with a realistic control model. They refer to tropical Pacific (TP), Indian (TI) and Atlantic (TA), but significant lower means were observed only in the latter.

The weaker MOC leads to significant colder SSTs in the North Atlantic, with important consequences on North American and European climate. So tropical Sea Surface Temperatures may impact extra-tropic regions not only by atmospheric teleconnections (as for atmospheric gyres, where a pattern of sub-tropical circulation has its opposite, weaker counterpart in the sub-poles) but also through affecting oceanic circulation in remote basins.

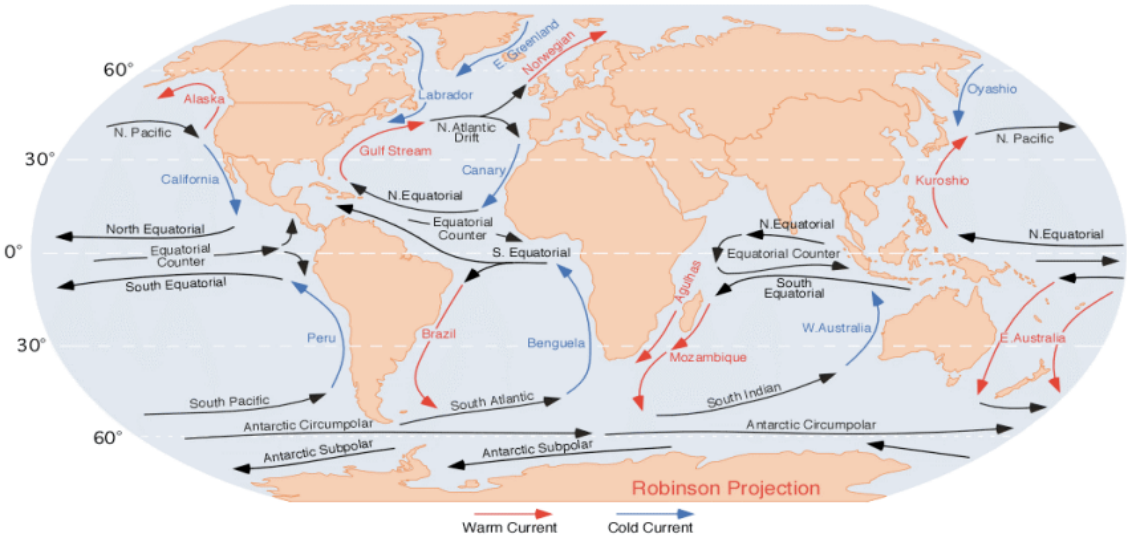

Figure 2.2: Dynamic flow of global ocean circulation patterns.

2.4 Internal variability

While external climate forcing derives from factors outside the climate system, internal variability arises from interactions and feedback mechanisms operating within it.

It manifests as short-term fluctuations in temperature, precipitation, wind patterns, and other climatic parameters, which can be observed on timescales ranging from months to decades. Internal variability can significantly impact short-term climate fluctuations, leading to periods of warmer or cooler conditions that may deviate from the long-term trends. This variability has implications for agriculture, water resources, ecosystems, and other sectors dependent on climate.

2.4.1 Upwelling

Upwelling is a natural phenomenon that last from several days to weeks, where deep, cold and rich in nutrient waters from the ocean's depths ($\geq$ 100m) are brought to the surface, caused by a combination of wind patterns and the Earth's rotation. Depending on the region, there exist coastal, equatorial or ice-land upwelling. Upwelling regions are important sources of marine productivity, as they attract hundreds of species at different trophic levels to create biodiversity hot spots.

Seawater is largely incompressible. Hence, the vertical volume flux induced by upwelling is only possible if the same volume of water per unit time is moved away laterally from a region by a divergence of the horizontal flow. In the case of equatorial upwelling, the surface Ekman drift at the equator, under the permanent easterly trade winds, creates a divergence that is balanced by a convergence of geostrophic

flow due to the east-west pressure gradient along the equator. Because the vertical distribution of the two meridional flows is different, a strong vertical circulation results [24], with superficial waters being replaced by sub-surface waters. Given that the upwelled water is generally heavier, so denser, than the water it replaces, the associated increase in potential energy of the system requires an external energy source, which is provided by surface wind stresses.

The variability of the wind is much stronger on time scales of a month or less than the annual period. Consequently, the observed upwelling events must be considered as a local response to winds of limited duration.

Ocean upwelling rates are difficult to measure because of the relatively small velocities involved, and therefore are typically inferred from indirect methods such as heat budget estimates and tracer observations. Such tracers derive from the presence, in surface water, of properties characteristic of thermocline water, which have been emplaced by the upwelling process. Examples include surface anomalies in C^{14}, C^{13}, He, CO_2, and lower Sea Surface Temperature [16].

In response to surface temperature increase due to global warming, it is hypothesized that the land–sea temperature gradients will enhance increasing upwelling favorable winds, with greater upwelling intensity and duration at higher latitudes. This could enhance the water stratification and negatively affect the concentration of nutrients, altering marine ecosystems; however the argument is still matter of discussion [11].

2.4.2 Thermocline shoaling

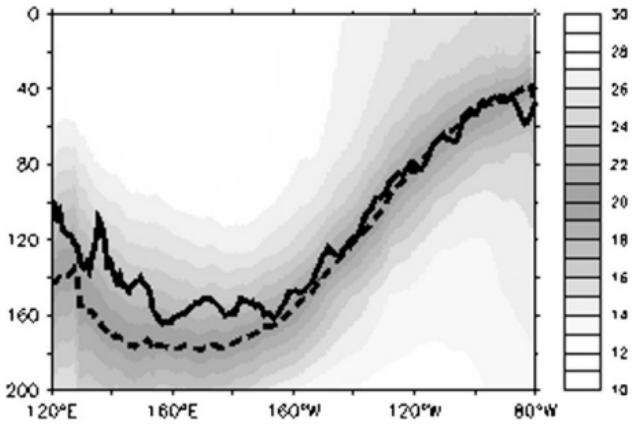

Figure 2.3: Climatological annual mean upper-ocean temperature (°C) averaged between 58S and 58N. The dashed line shows the location of the 20°C isotherm (Z_{20}), and the solid line shows the location of the maximum vertical temperature gradient (Z_{tc}).

The shoaling of the thermocline indicates a process where the thermocline,

namely the layer in the water column where there is a rapid change in temperature, moves closer to the surface.

At the Equator, an increase in the wind stress due to the east-west SST gradient results in a drop of sea level, leading to the uplift of subsurface isotherms and reduced Sea Surface Temperature. So the intensity of thermocline uplifting can be also considered an index of equatorial upwelling.

The thermocline depth (DTC) is defined as the depth of the maximum vertical temperature gradient (Z_{tc}). Thus, the DTC is often determined by the depth of a representative isotherm (e.g., the depth of the 14° or 20°C isotherm, Z_{14} and Z_{20}, respectively) within the thermocline layer [25]. The Z_{20} is suitable for the warm pool in the western equatorial Pacific, but it may fail for the cold tongue in the eastern region and coastal upwelling regions, because the 20°C isotherm may outcrop to the surface during the cold season. On the other hand, the Z_{14} is too deep to represent the warm pool thermocline temperature.

The DTC is defined by averaging 12°C (representing the temperature at the base of the thermocline layer) and the local long-term mean Sea Surface Temperature. Z_{tc} varies from 20.5°C in the warmest places to about 16°C near the Peru coast. The Z_{tc} and Z_{20} in the equatorial Pacific generally coincide with each other (Fig.2.3, [25]), except in the warm pool region where the Z_{tc} is shallower than the Z_{20} by about 20–40m.

2.4.3 El Niño Southern Oscillation

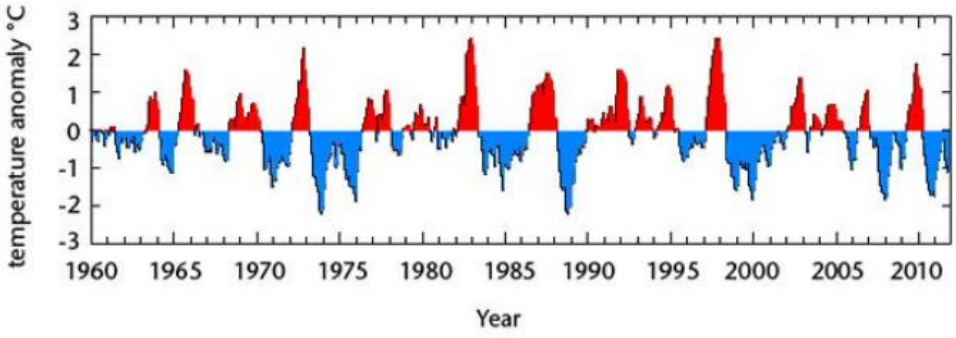

Figure 2.4: Monthly SST anomalies in a region of the central equatorial Pacific that indicates the rotation of El Niño (red) and La Niña (blue) episodes. Source: Met Office UK.

The El Niño-Southern Oscillation (ENSO) is natural a recurring climate pattern that has been active for thousands of years, involving changes in the temperature of waters in the central and eastern tropical Pacific Ocean.

On periods ranging from about three to seven years, the surface waters across a large swath of the tropical Pacific Ocean warm or cool by anywhere from 1°C to

3°C, compared to normal. While the global climate system contains many processes, ENSO is by far the dominant feature of climate variability on inter-annual and decadal time scales. It directly affects rainfall distribution in the tropics and can have a strong influence on weather across the United States and other parts of the world.

El Niño and La Niña are the extreme phases of the ENSO cycle. The term "Southern Oscillation" refers to the atmospheric pressure changes between the east and west tropical Pacific. Such events are a consequence of strong and extensive interactions between the ocean and atmosphere and they are associated with widespread changes in the climate system that last several months.

Specifically, El Niño indicates an anomalous sustained warming of the ocean surface, meaning above-average Sea Surface Temperatures, in the central and eastern tropical Pacific Ocean. Over Indonesia, rainfall reduce while increases over the central and eastern tropical Pacific Ocean. The low-level surface winds, which normally blow from west to east along the equator ("easterly winds"), instead weaken or, in some cases, start blowing the other direction as "westerly windbursts", short-lived storm-like events in the western Pacific that disturb the 'balance' maintained by easterly winds.

On the other hand, during a 'La Niña' event, a cooling of the ocean surface, or below-average SSTs in the central and eastern tropical Pacific Ocean are observed. Over Indonesia, rainfall tends to increase while decreasing over the central and eastern tropical Pacific Ocean. A La Niña event can arise similarly to El Niño, with the outgrowth of normal easterly winds along the equator.

In general, the more pronounced the temperature anomalies, the stronger the intensity of El Niño or La Niña events (and vice-versa).

Definitions vary, but as a guide the El Niño and La Niña episodes occur when anomalies in this region are larger than about 0.5 °C in magnitude for several months. A typical episode might last for three or four seasons, peaking in size in boreal winter, but events are not entirely regular and have various sizes and duration. The climate system does not always simply alternate between El Niño and La Niña: the same type of event can occur successively or be sustained over several years, or a third phase called ENSO-neutral can manifest, when neither or the two occurs.

The ENSO cycle is illustrated in the figure 2.4 by a time-series of the monthly SST anomalies in a region of the central equatorial Pacific. The number and intensity of El Niño events have significantly increased during the latter half of twentieth century (12 events), in comparison with the former half (7 events). During recent decades, SST anomalies exhibits more positive values in the eastern Pacific [8].

Chapter 3

Trend Analysis and Observations

The aim of this Chapter is to recognize some pattern in the evolution of SSTs trends over the XX century. Noting that on the Earth general warming has been observed, one may expect to find some form of positive trends. The HadISST data set has been analyzed using the Zapata library for Python, developed by the Euro-Mediterranean Centre on Climate Change (CMCC). As said before, the HadISST data set consist in a three dimensional grid (latitude, longitude and time) of monthly mean global Sea Surface Temperature, from 1870 to 2020. So it is possible to depict every monthly mean on a geographical map as seen in 3.1.

To evaluate long time scale variations, the 150 years long SST time series has been divided into five periods of 30 years; trends have been computed on each grid point performing linear regression on each of them, and then represented on geographical maps (Fig. 3.4, 3.5, and 3.6).

3.1 Geographical SST trends

The first remarkable feature is that the global mean SSTs have increased since the beginning of the records in 1870 and that the magnitudes of warming trends in the last 30 years are more significant than at the beginning of the XX century. These are the region of particular interest that display warming or cooling trends, that are going to be discussed with further details:

1. the Northern Pacific has experienced a warming trend, more enhanced along the Asian and American coast, except for the period 1960-1990, where an offshore cooling was registered;

2. in the last 60 years the Equatorial Pacific has been characterized by a SST gradient defined by an equatorial cold tongue at east and a warm pool at west;

3. in the Northern Atlantic there is a strong north-south SST gradient, that extend from the coast of Greenland to the northern American east coast, which has been increasing since the 1930s;

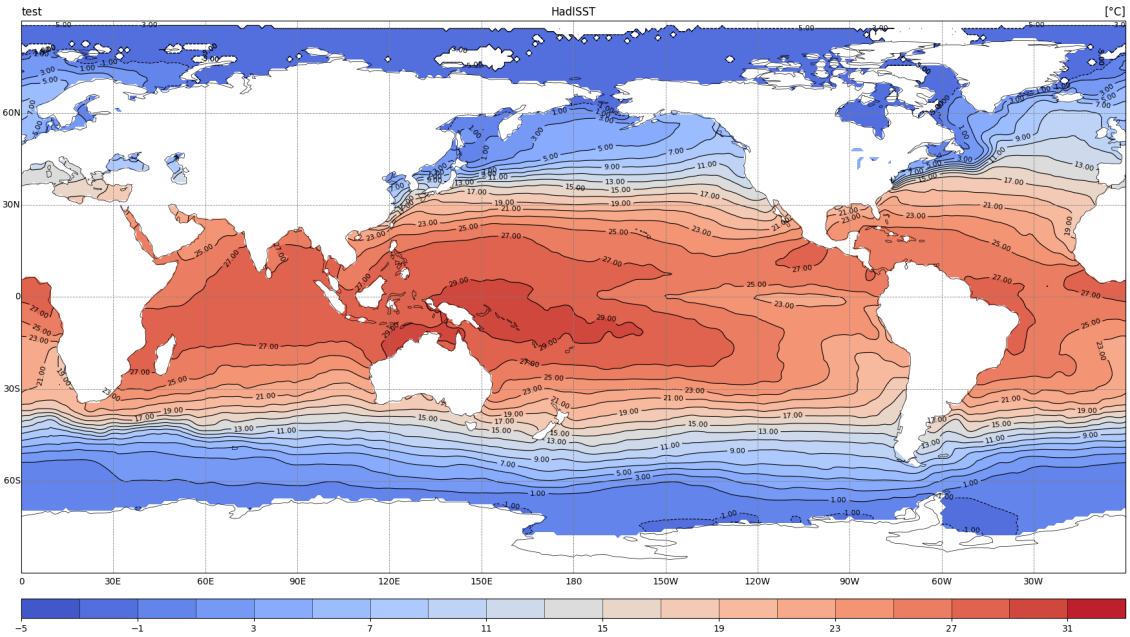

Figure 3.1: Monthly mean SST grid for January 1870 from the HadISST data set.

4. the Indian Ocean generally warmed, more rapidly in the last 30 years.

3.1.1 Northern Pacific Ocean

In the past 150 years, the SST in the northwest Pacific has been increasing. In the past 30 years, the SST trends have reached 0.035°C/30 years, stronger in the coastal region than in the ocean and deep-sea region.

There exist decadal to multidecadal variations in the SST trends, with a general cooling period from the 1870s to the 1900s, a weak warming period from the 1900s to the 1930s, a weak cooling period from the 1960s to the 1990s and a recent warming period from the 1990s to the present.

Observations and numerical simulations show that large scale SST anomalies of over 20° in longitude and latitude can cause significant variations in atmospheric circulation that results in upwelling variations [10], related to the increase of the vertical stratification of the water and changes in the intensity and period of coastal winds. So the northwest Pacific determines the oceanic climate change in China, which will have an impact on the marine environment in Chinese coastal areas, causing land-based droughts, floods and climate disasters.

3.1.2 Tropical Pacific Ocean

From the second half of the last century onwards, in the Tropical Pacific two pronounced north-south and east-west gradients formed. Although the global SSTs

have generally increased throughout the XX century, a narrow band on the eastern equatorial region didn't warm as it may be expected. In Fig. 3.5(b) and 3.6 it is shown that the trend of Sea Surface Temperature stayed close to zero or was even negative.

Considering the period from 1958 to 2018, the 95% confidence level t-test performed (see Appendix A) proved that in the cold tongue there is no statistically significant warming trend.

The Tropical Pacific influences weather worldwide and responds to the rising of greenhouse gases (GHGs) impacting biodiversity, natural environments, society and economics, so climatologists are trying to understand the reasons behind this anomalous behaviour, especially since, how it will be discussed in the next Chapter, the state-of-the-art climate models still show large errors.

The debate around the reason of equatorial Pacific cooling is still open, and according to Olonscheck et al. [20] the observed trends might be within the range of model simulation once internal variability is taken into account, as observed and simulated trends in SST patterns are broadly consistent, and the latter can explain the major pattern of variability when considering period of 30 and 20 years.

Otherwise, according to Seager et al. [9], SST trends are at the very extreme cold limits of modern simulations, however it is still possible to explain the existence of the cold tongue and the east-west SST gradient using fluid dynamics, thermodynamics and taking into account the rising of GHGs.

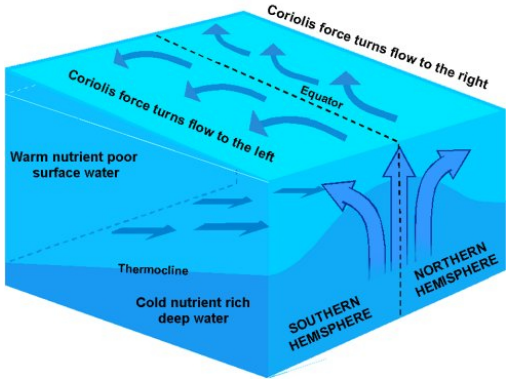

Figure 3.2: Equatorial upwelling and thermocline shoaling.

The cold tongue is positioned over the Intertropical Convergence Zone (ITCZ), an area where northeast and the southeast trade winds converge. These drive water westward, creating high sea level and a deep thermocline in the west, and low sea level and a shallow thermocline in the east, while the Ekman transport causes upwelling that enhances the temperature gradient. This results in a narrow cold tongue at east and a warm pool at west. The coupled atmosphere–ocean process is such that the mean temperature will increase less than it would with the purely thermodynamic response.

Wind-driven variation of the thermocline depth allows oscillation between El Niño and La Niña events on interannual to longer time scales. During the warm El Niño phases of the ENSO, the SST gradient and easterly winds weaken, and deep convection, namely vertical atmospheric motion of convection that extend from near the surface to above the 500 hPa level, transfer from the warm pool to east. Weakened easterlies, in turn, reduce upwelling causing warming, and the weaker SST gradient further weakens the easterlies.

As greenhouse gases increase in the atmosphere due to anthropogenic causes, they enhance the natural greenhouse effect: these gases trap more heat in the lower atmosphere, leading to a rise in overall atmospheric and ocean's surface temperatures as well. When warm surface waters are carried westward by ocean currents and evaporate, they, in their turn, release heat into the atmosphere. As the ocean's surface warms, it can affect the solubility of gases: warmer waters have a reduced capacity to dissolve gases, leading to a decrease in the ocean's ability to absorb excess carbon dioxide from the atmosphere. Equatorial Pacific is then the largest source of CO_2 from the ocean to the atmosphere [21].

Consequently, the warming of the ocean surface can lead to changes in ocean currents and atmospheric circulation that can disrupt the typical temperature patterns.

According to previous studies [2], it is possible that the cold tongue is slowing global warming: on decadal time scales, an overall stronger than normal SST gradient since 1998 has driven dry conditions in western North America and East Africa, and temporarily reduced the rate of global warming in the atmosphere by enhancing the rate of ocean heat uptake [9]. Furthermore, upwelling and shallow thermocline allow some of the heat added by GHGs to be diverged away such that the cold tongue warms less than the warm pool, strengthening the zonal SST gradient and, hence, the trades. This cold hiatus is probably temporary, and global warming will return when the tropical Pacific swings back to a warm state [18].

3.1.3 Northern Atlantic Ocean

A region of enhanced warming off the northeastern coast of North America, and a region of cooling to the south of Greenland are very noticeable especially since the 1960-1990 period (Fig. 3.5, 3.6). It is estimated that the coast of Greenland has been cooling by about 1°C since 1870, while nearby, along the northeastern coastline of North America, the ocean surface has been warming much faster than the global ocean on average, by about 1.5°C since 1870 [17], creating an anomalous horizontal SST gradient of considerable magnitude. This feature, referred as 'Cold Blob' or North Atlantic warming hole by the scientific literature, is in contrast with the global mean warming trend and has been associated with recent marine heatwaves, generating substantial economic and ecosystem impacts [17].

Many of the ways in which the atmospheric circulation has changed, and is expected to change, in response to anthropogenic radiative forcing, are attributed to

global energy imbalances. It has been hypothesized that the rising atmospheric CO_2 concentration resulted in long-term changes in the buoyancy-driven ocean circulation, namely a slowdown of the Atlantic Meridional Overturning Circulation, rather than being driven by, or coupled to, pure surface wind forcing.

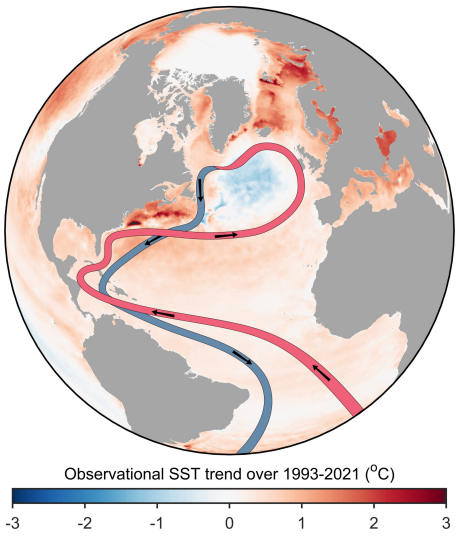

Figure 3.3: Atlantic MOC and SST trends over 1993-2021. The strong north-south SST gradient is visible.

Ceaser et al. [1] demonstrated the correlation between the variation of the Atlantic MOC extent and this SST anomalies, finding a cause effect relationship, or "fingerprint", of these correlated behaviour. Reconstructed data suggest an AMOC trend of -1.7Sv per century; the fingerprint consists of a cooling in the subpolar gyre region due to reduced heat transport, and a warming in the Gulf Stream region due to a northward shift of the Gulf Stream. This fingerprint is most pronounced during winter and spring, and it is found in the observed long-term temperature trends, indicating a pronounced weakening of the AMOC since the mid-twentieth century. The AMOC weakening may already have an impact on weather in Europe. Cold weather in the subpolar Atlantic correlates with high summer temperatures over Europe, and the 2015 European heat wave has been linked to the record 'cold blob' in the Atlantic that year. Model simulations suggest that this event is very likely to be largely anthropogenic, given that it emerges in response to rising CO_2 levels; moreover, an AMOC weakening could potentially lead to increased storminess in Europe. Continued global warming is likely to further weaken the AMOC in the long term, via changes to the hydrological cycle, sea-ice loss and accelerated melting of the Greenland Ice Sheet, causing further freshening of the northern Atlantic.

Karnauskas et al. [17] studied the atmospheric response to this SST trends and demonstrated through a coupled atmospheric-ocean model that, other than affecting mid-latitude events in seasonal time scale, namely a local deceleration of the westerlies combined to a low Sea Level Pressure (SLP) in the eastern northern Atlantic during the boreal winter, this anomaly also induce effects that propagates on global scale.

Horizontal stationary Rossby wave flux, namely stationary waves characteristic of a rotating fluid that propagate on a planetary scale, establishes the direct link between the anticyclone in the North Atlantic and the cyclone over the Arabia Sea and India, which manifests as a low SLP anomaly at the surface. The resulting

anomalous meridional SLP gradient in the Indian Ocean drives a northward surface wind anomaly that weakens the Asian-Australian winter monsoon, shifting northward the the Intertropical Convergence Zone. The northward shift of the Indian Ocean ITCZ is particularly robust in boreal winter, but is present year-round.

3.1.4 Indian Ocean

The central-eastern Indian Ocean is characterized by Sea Surface Temperatures greater than 28.0°C and also an increased warming over the Indian Ocean during the past 60 years has been registered (Fig. 3.5(b) and 3.6), although the reasons behind this monotonous warming are still debated.

Studies reveal that the western tropical Indian Ocean has been warming at a faster rate than any other region of the tropical oceans, and turns out to be the largest contributor to the overall trend in the global mean Sea Surface Temperature [8].

In Fig. 3.6 an east-west temperature gradient is noticeable. At the beginning of the XX century, the mean summer SST over the western Indian Ocean was around 26.5°C, cooler in comparison to the rest of the Ocean. Today it has reached 28°C. The heating of the typically cooler western Indian Ocean in comparison to the rest of the warm tropical pool area modifies the horizontal Sea Surface Temperature differences, which could potentially lead to shifts in the circulation and precipitation patterns of the Asian monsoon, and also drastically change the convective response from shallow to deep convection [8].

Furthermore, this occurrence has the potential to induce modifications in the marine food chains within this ecologically diverse zone. The western Indian Ocean stands out as a highly fertile area particularly during the summer due to its pronounced upwelling. A a substantial shift in the SSTs in this locality could also disrupt marine food webs.

Besides direct contribution from greenhouse warming, the long-term warming trend over the western Indian Ocean during summer is highly dependent on the asymmetry in the El Niño–Southern Oscillation teleconnection, and the positive SST anomalies associated with ENSO during recent decades. As said in Section 2.4.3, the last five decades saw the most intense and frequent El Niño events, opposing to more modest La Niña episodes. Apart from the direct radiative forcing due to increasing greenhouse gases, El Niño appears as an event through which the Pacific Ocean throws out its heat, which partially gets accumulated in the Indian Ocean. Although the frequency of El Niño events has increased in the recent decades, a strong warm event has not been recorded since 1997/98, and correspondingly the Pacific and Indian Ocean SST anomalies show a slight dampening.

3.1.5 Effects on SST

The mechanisms described above have direct consequences on SST trends, that displays correlated anomalies. For instance, climate change will affect atmospheric circulation, leading to increasing SST trends in the coastal northwest Pacific. Because rising greenhouse gases are connected to higher SST, but at the same time upwelling events and thermocline shoaling are capable to slow heating locally, we expect to observe a north-south and east-west SST gradient in the equatorial Pacific. In the northern Atlantic the MOC weakening will determine cooling SST in the subpolar region and warming over the northern American coast, the latter being connected to the shift of the Gulf Stream. Since these phenomena are driven by the rising CO_2, we expected that both this regions will intensify their temperature contrast over the course of the XX century. Finally, the effect of global warming combined to the intense El Niño events of the last 50 years will determine a considerable warming over the Indian Ocean.

3.2 Results and Observations

The five periods show alternating phases of warming and cooling trends, with increasing magnitude and rapidity of warming over time. Here the variations of trends over the five thirty-year periods from 1870 to 2020 are summarized:

1. 1870-1900 (Fig. 3.4(a)). SST doesn't display many significant trends, except the areas that extends from the southern American east coast to the Equatorial Pacific, the Asian and American Northern Pacific coast, the Indian western warm pool and some coastal Atlantic zones, where the warming is less than 0.6°C;

2. 1900-1930 (Fig. 3.4(b)). Here the Equatorial Pacific shows an inversion of the trend with cooled or constant SST (down to −0.3°C). Wider regions over the northern Pacific and Atlantic Oceans and the Mediterranean Sea undergoes warming (+0.3°/0.75°C);

3. 1930-1960 (Fig. 3.5(a)). Pronounced warming (+0.9°/2.4°C) in the Northern Pacific is shown, while the Equatorial region continues to cool down (−0.45°/0.75°C) and the north-south northern Atlantic gradient intensifies (−1.35°C as opposite to +1.8°C);

4. 1960-1990 (Fig. 3.5(b)). In the Pacific, the cooling trend narrows in a "cold tongue" of constant SST and the east-west temperature gradient enhances (up to +0.45°C in the warm pool), the Indian Ocean warms considerably (+0.3°/0.75°C) while the offshore northern Atlantic is characterized by a cooling trend (−0.1°/1.2°C);

5. 1990-2020 (Fig. 3.6(a)). During the last 30 years, the magnitude of warming shifted to higher temperature in the Pacific, Atlantic and Indian Ocean (+0.45°/1.5°C) except for the cold tong, which maintained relatively low SST, a strong north-south gradient in the Equatorial Pacific, and the intensified gradient in the northern Atlantic (−0.15°opposite to +2.4°C).

As mentioned before, according to Seager et al.[9][21], the est-west and north-south SST gradients in the equatorial Pacific, namely the clear distinction between a region that maintained constant temperature through the last 60 years, and the adjacent warmer zones, are driven primarily by the rising of GHGs, which concentration has risen sharply during this period of time.

The trends shown by the HadISST data set, especially those from the periods 1960-1990 and 1990-2020, confirm the lack of warming in this equatorial band, as opposed to the neighbouring regions at north, south and west, where SST increased considerably through time.

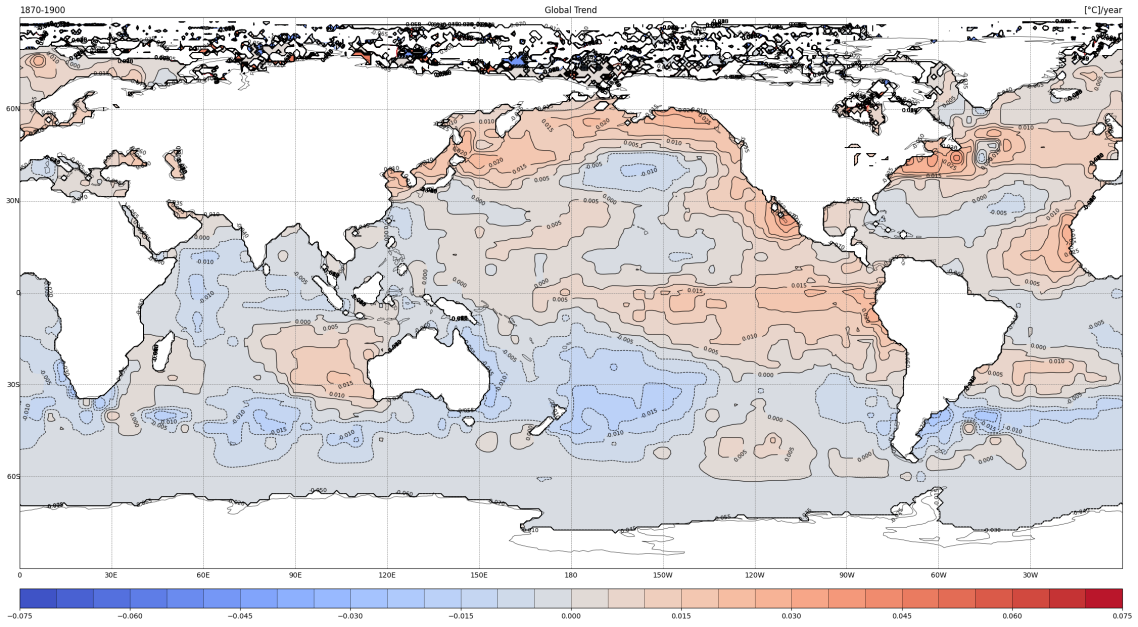

(a)

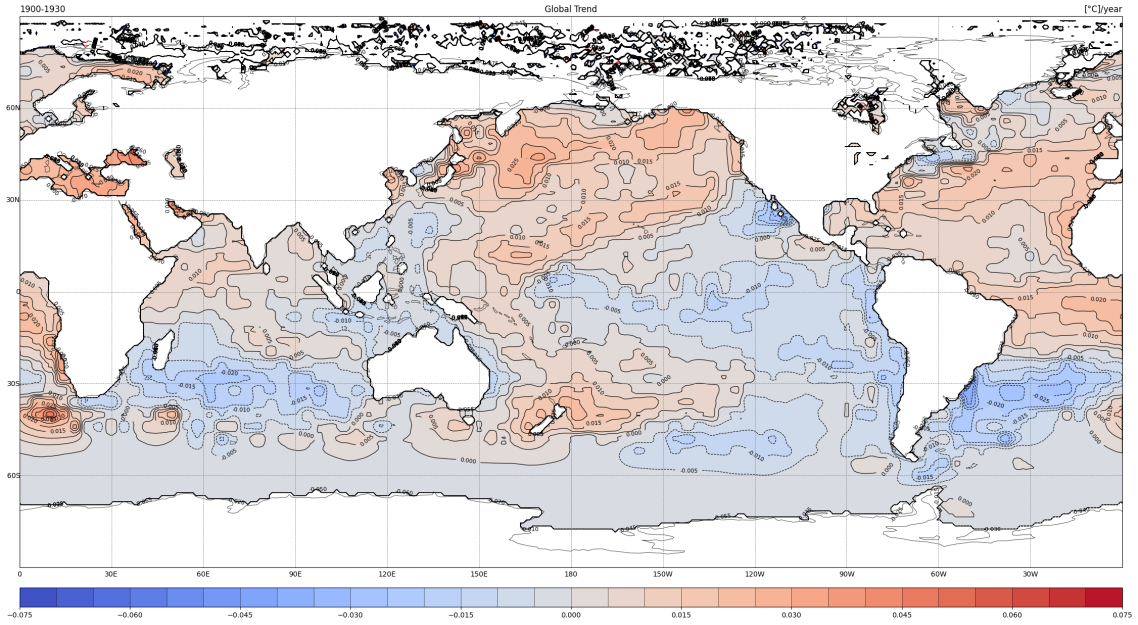

(b)

Figure 3.4: Global SST trends over the course of the periods (a) 1870-1900 and (b) 1900-1930. The scale refers to the variation of 1°/30y.

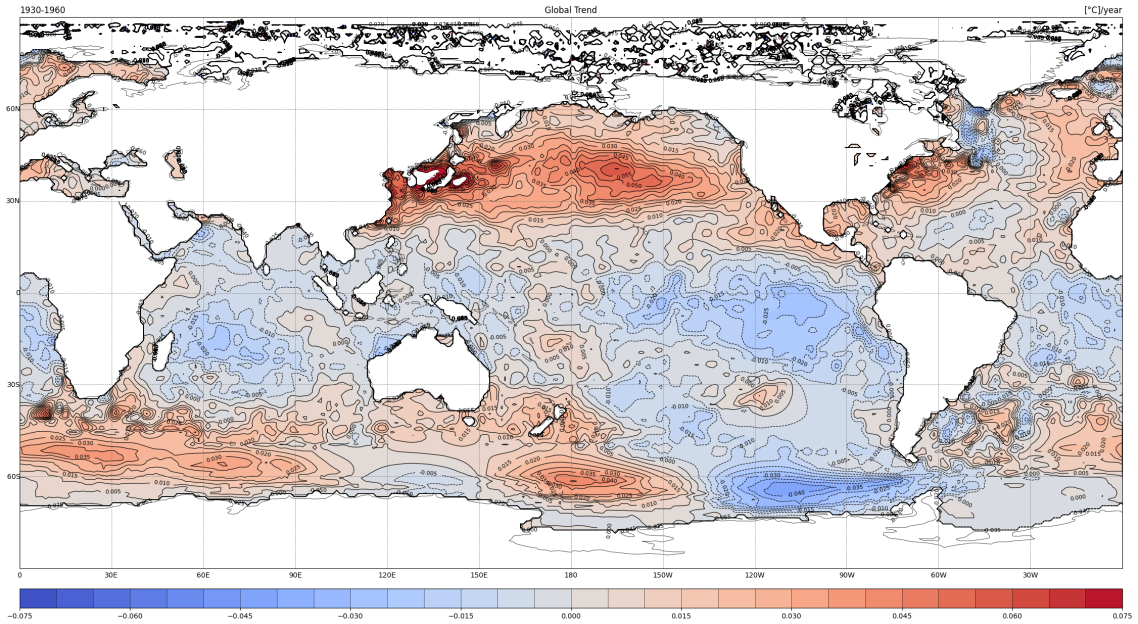

(a)

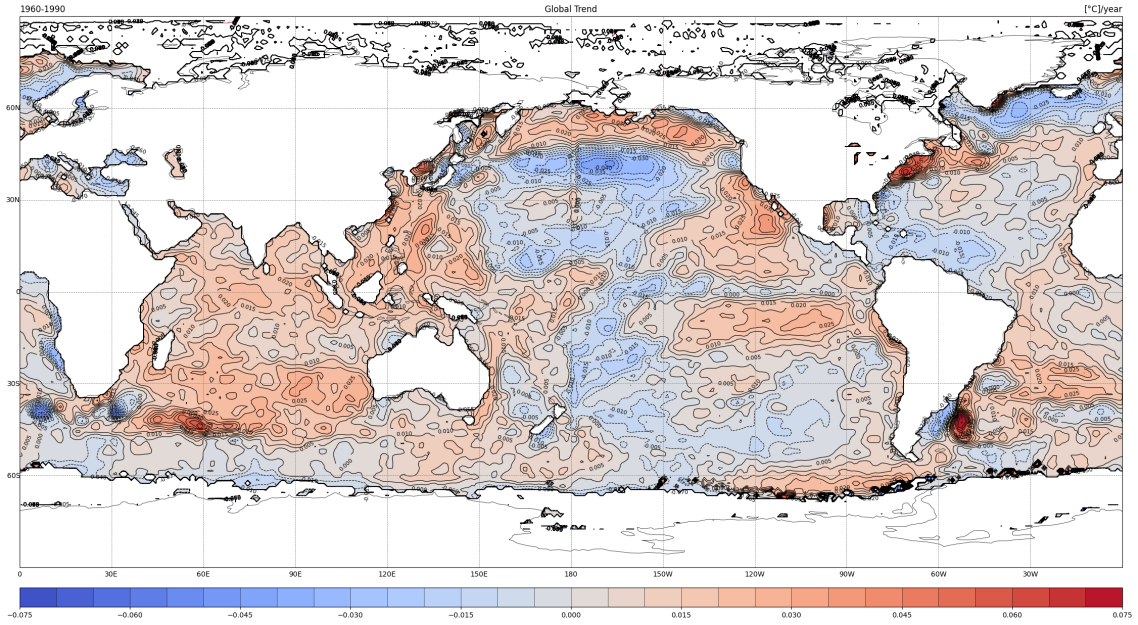

(b)

Figure 3.5: Global SST trends over the course of the periods (a) 1930-1960 and (b) 1960-1990. The scale refers to the variation of 1°/30y.

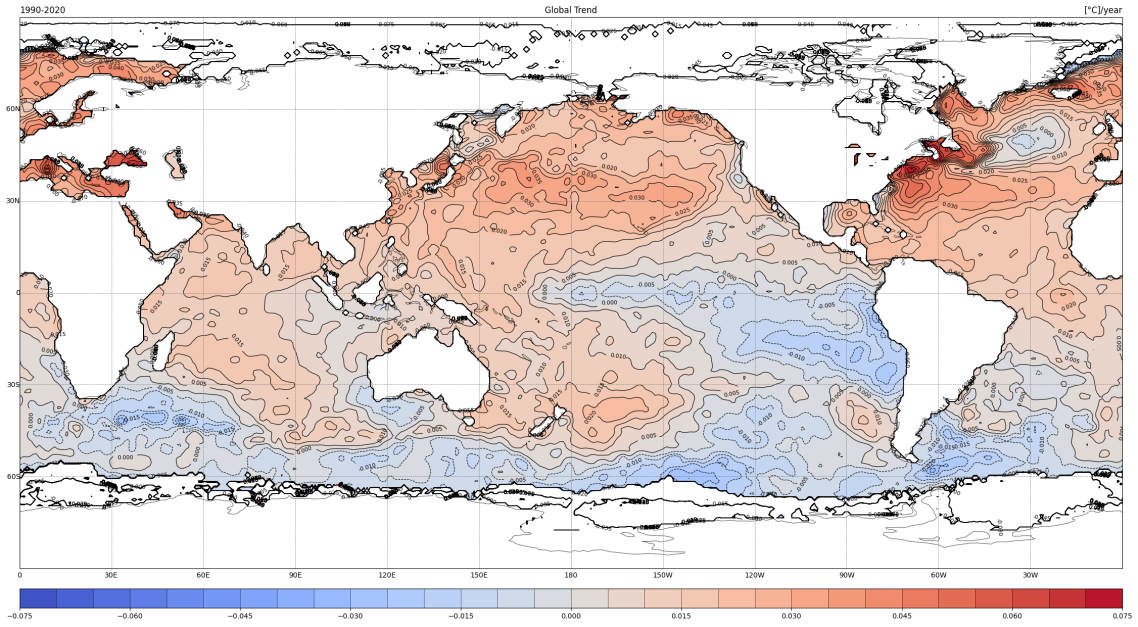

(a)

Figure 3.6: Global SST trends over the course of the period 1990-2020. The scale refers to the variation of 1°/30y.

Chapter 4

Numerical Climate Models

The scientific community agrees that over the course of the XX century the Earth surface temperature has increased from $\sim 0.3^{\circ}$ to 0.6°C [2], mostly due to anthropogenic activities, but the role of the forced versus internal response is still under investigation. General Circulation Models (GCMs), namely mathematical representations of the atmosphere, oceans, land surface, and other components of the Earth's climate and their interactions, still show errors in the reproduction of the SST trends.

This Chapter discuss the state-of-the-art models capacity to reproduce SST trends over the XX and XXI century presenting some of the current projects and institutions about climate modelling. The HadISST is then going to be compared with the CMCC-CM2 historical trend simulation and with the ensamble of simulations performed by Seager et al.[21].

4.1 Numerical Models

The aim of numerical models is to simulate and when possible predict weather and climate phenomena basing on primitive laws such as the conservation of mass, the Navier-Stokes equations and laws of thermodynamic. Numerical models can differ in terms of spatial domain and resolution as well as the time period for which the forecast is valid: for instance, Numerical Weather Prediction Models (NWP) are used primarily for weather forecasting, while global General Circulation Models (GCM) are used to make predictions on seasonal to decadal time scales. To account for uncertainty in the initial conditions, many simulations, with slightly different initial conditions are performed to create a statistical ensemble.

The atmospheric module within a GCM is its most intricate part; it uses fundamental equations to replicate the progression of variables like wind speed and direction, temperature, humidity, and air pressure. GCMs additionally encompass equations that depict oceanic circulation, illustrating heat transport and the interchange of heat and moisture between the ocean and atmosphere. These models also

include land surface and the cryosphere.

For computational analysis, GCMs divide the atmosphere, oceans, and land into a three-dimensional grid structure. Subsequently, the equations are numerically computed within each grid cell at successive time intervals covering the simulation's duration. The quantity of cells in the grid establishes the model's resolution or level of detail. Each grid cell is characterized by average values of corresponding variables, consistent attributes like velocity, temperature, and others. The finest spatial resolution achieved thus far for climate simulations is 0.5 degrees (equivalent to 60 kilometers at the equator), but there are underway attempts to reach much higher resolutions, up to a kilomnetric scale.

A major source of uncertainty when making climate projections over decades is the difference between sunlight energy absorbed by Earth and the energy radiated, or reflected, back into space, induced by anthropogenic greenhouse gases (GHGs) emissions. This is called radiative forcing, and equivalently to the forcing seen in Chapter 2, it has an impact on the global climate. GHG emissions depend largely on the usage of fossil fuels and thus human behavior. To cope with this uncertainty, the climate research community makes use of a suite of several emissions scenarios called Representative Concentration Pathways (RCP). Each RCP represents a potential trajectory of atmospheric GHG concentrations over the coming decades, culminating in a specific excess radiative forcing at the year 2100. The RCP8.5 scenario, for example, assumes high and growing emissions that will lead to an 8.5 W/m^2 extra radiative forcing in the year 2100 and an average increase in surface temperatures of between 2.6°C and 4.8°C [15].

To determine whether the occurrence of extreme events will change over the next decades, large ensembles are needed, as such events are by definition rare. Several studies indicate that the probability distribution of extreme events will change as Earth's climate continues to warm. In the case of annual maximum temperature, for example, in many continental-scale regions the mean is shifting to an higher temperature while the amplitude of the positive tail of the distribution increases.

4.1.1 The Coupled Model Intercomparison Project

The Coupled Model Intercomparison Project (CMIP) is an international project that involves multiple research institutions, climate modeling centers, and scientists from around the world. CMIP experiments have gone through multiple phases of refinement, of which the last is CMIP6. The purpose for which CMIP was developed was to solve a series of issues, such as how does the Earth system respond to forcing, what are the origins and consequences of systematic model biases and how to assess future climate changes given internal climate variability, predictability, and uncertainties [5].

Historical forcings are based as far as possible on observations; they provide rich opportunities to test model ability to simulate climate. These include: GHG concentrations and emissions, solar forcing, stratospheric aerosol deriving from volcanoes,

Sea Surface Temperatures and Sea Ice Concentrations.

The behavior of CO_2 and other GHGs in the atmosphere are simulated considering their concentration, distribution, and interactions with other atmospheric components, and also taking into account physical and chemical processes that govern the behavior of CO_2 in the atmosphere, such as absorption, scattering, and re-emission of infrared radiation. CMIP models project future climate conditions under different emission scenarios simulating various feedback mechanisms as CO_2 concentrations increase due to emissions: rising temperatures, changes in cloud cover, ice melting, and other processes that can amplify the effects of CO_2-induced warming.

4.1.2 The Large Ensamble Community Project

The Large Ensemble Project (LENS), unlike traditional climate models that run a single simulation or a small number of simulations, includes a 40-member ensemble of fully-coupled simulations for the period 1920-2100.

Each member is subject to the same radiative forcing scenario RCP8.5, but begins from slightly different model parameters or initial atmospheric states created by randomly perturbing temperatures at the level of round-off error. Then, after losing the memory of initial condition (usually in a couple of weeks) each ensemble member evolves chaotically, affected by atmospheric circulation fluctuations characteristic of a random, stochastic process.

All simulations are performed with the nominal 1°latitude/longitude version of the Community Earth System Model version 1 (CESM1). The Large Ensemble Project also includes a set of multi-century control simulations with the atmosphere, ocean, and fully-coupled versions of CESM1 under pre-industrial (1850) radiative forcing conditions (2600 years, 900 years and 1800 years in length, respectively) [6].

4.1.3 The CMCC Climate Model 2

The Euro-Mediterranean Centre on Climate Change coupled Climate Model Version 2 (CMCC-CM2) [3] is a family of climate models developed at CMCC that realistically represent patterns of temperature, precipitation and winds, that contributed to CMIP5 and CMIP6.

The CMCC-CM2 model components are full 3-D dynamical models, communicating via a coupler that synchronizes the exchange of fields among the different model constituents. The components of the coupled model are the Community Atmosphere Model, the NEMO ocean engine, the Community sea-Ice CodE (CICE) and the Community Land Model.

In CMCC-CM2 all model components have a coupling frequency of 30 min, except for the ocean that exchanges coupling fields every hour (equal to the relative integration time step). The atmosphere sends to the coupler information about zonal and meridional velocities, atmospheric temperature and humidity, including

precipitation, and downward shortwave and longwave radiation. It receives from the coupler status of the surface albedo, land/ice/ocean fractions, Sea Surface Temperature, surface wind stresses, sensible and latent heat fluxes, upward longwave radiation, evaporation, and dust emissions.

4.2 Shortcomings in SST modelling

Notwithstanding the advances, climate models still have systematic errors that are less relevant in investigating the response to changes in forcings, since the errors will somewhat subtracted in the differential simulations, nevertheless the effort is continuous to improve and remove such systematic errors. We are focusing here on the ability of the model to capture the SST trends. Particularly interesting is the equatorial cold tongue upwelling region: here the thermocline shoaling and lack of warming, and the east–west and north–south SST gradients seem to be at the very extreme, or beyond, the modeled behavior. Given the critical role of the equatorial Pacific in the global climate and carbon systems, the question raised, and still matter of discussion, is whether, and to what extent, the absence of positive temperature trends in the eastern equatorial Pacific is a consequence of internal variability, the rising of GHGs or both. It is important to know how in this region SSTs respond to rising greenhouse gases in order to predict the future global climate.

A study conducted by Seager et al. [21] uses collectively 511 simulations from CMIP6 and 6 LENS models to analyse Sea Surface Temperature over the period 1958-2018. For the same period, temperature trends have been computed from the HadISST data set and represented in Fig. 4.1(a). When evaluating the coherence of the simulation, three metrics have been used. The first is the differential warming between the warm pool region of the west and the cold tongue region, where the thermocline is shallow and the upwelling has important consequences on SSTs. It is positive if the SST gradient strengthens. The second metric measures the differential warming in the east between the equatorial upwelling region and the waters immediately to the north and south. It is positive for relative cooling at the equator. The third metric measures the similarity between observed and modeled trends across the entire equatorial Pacific.

If the observed lack of cold tongue warming is a result of natural variability, it would be expected that many of these simulations, which sample the model natural variability well, would produce it.

Instead, of all the LENS, only few can match the trends; in Fig. 4.1 the observed trends are compared to the multimodel means from CMIP6 and LENS. Clearly, they show a diffuse and homogeneous warming that doesn't match the observations. The GFDL-ESM2M (Fig. 4.2) model could appear quite realistic, noticing that the cold tongue and the warm pool are well represented. However, each individual models run from the ensembles has been ranked by the three metrics, equally weighted, [21] and it has been found that GFDL-ESM2M provides runs that were also among

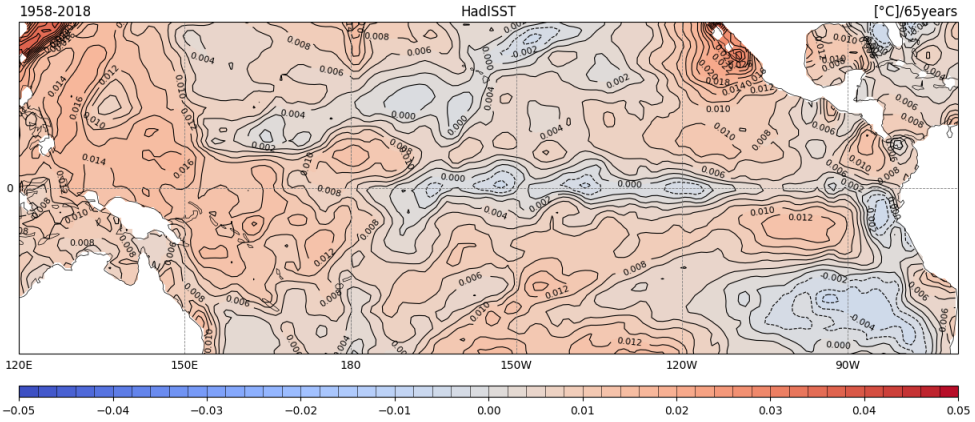

(a)

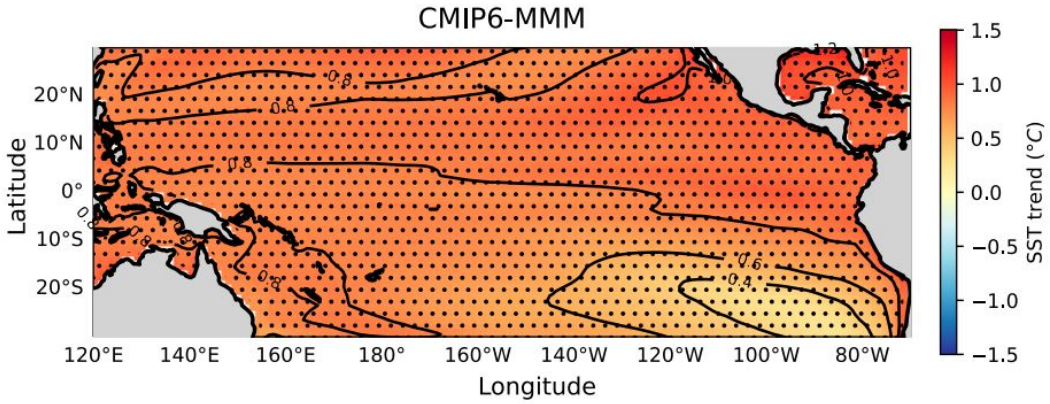

(b)

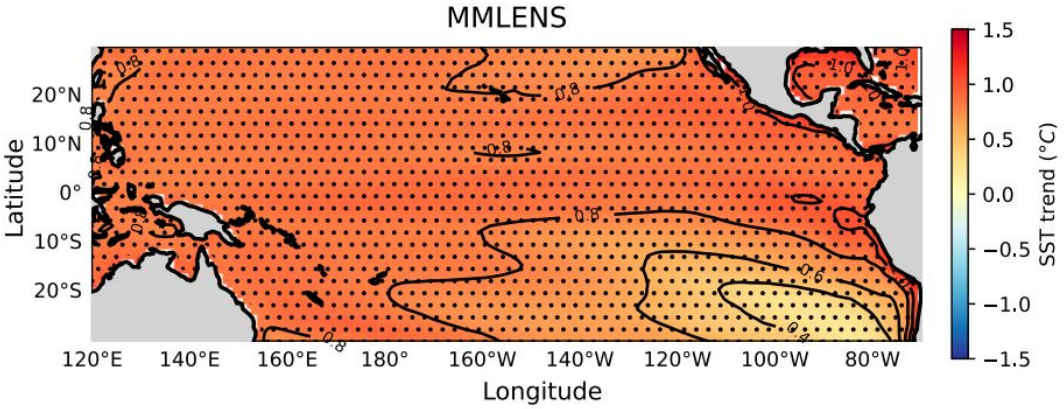

(c)

Figure 4.1: Comparison of the observed trend from HadISST (a) the CMIP6 multimodel mean (b) and the LENS mean (c).

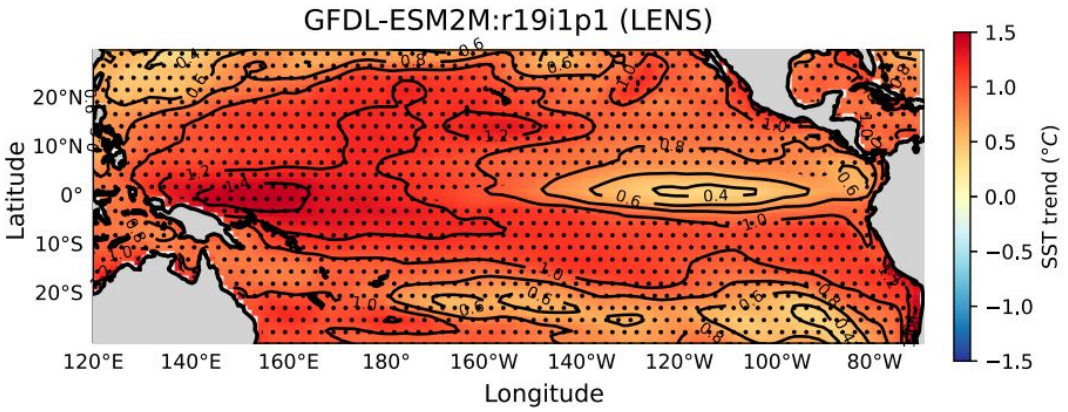

Figure 4.2: The GFDL-ESM2M from LENS. It displays some similarities to the HadISST trends, but because of the total runs, the matches are probable just a coincidence due to internal variability.

the lowest classified in terms of matching the observed trends, so the good match derives from model internal variability and it can't be considered consistent with forcing response.

From the study of the metrics mentioned above, it has been said that the east-west gradient is *extremely likely*, and the north-south gradient is *virtually certain*, to be outside the range of what CMIP6 and LENS can produce using internal variability and forced change. Namely the difference between trends on observations-based products and models cannot easily be explained away by appealing to the observations-based trend being strongly influenced by internal climate variability [21]. According to Seager et al. [9] the erroneous warming is a consequence of the bias of their equatorial cold tongues.

4.3 1950-2014 SST simulation

Here we use the simulation of the XX century of the coupled climate model CMCC-CM2 [3] to compute the simulated SST trends for the period 1950-2014 and it is then compared to the corresponding observation from the HadISST data set for the same period (Fig. 4.3), this is what is shown:

1. the east-west gradient that characterize the equatorial Pacific Ocean, creating a cold tongue of constant SST at east and a warmer pool at west, including a north-south gradient that surrounds the cold tongue, clearly visible in Fig. 4.3(a), is completely absent in CMCC-CM2 (Fig. 4.3(b)). On the contrary, the simulation looks to display the opposite SST trends, with warming at east (∼0.8-1K) and a null trend at west;

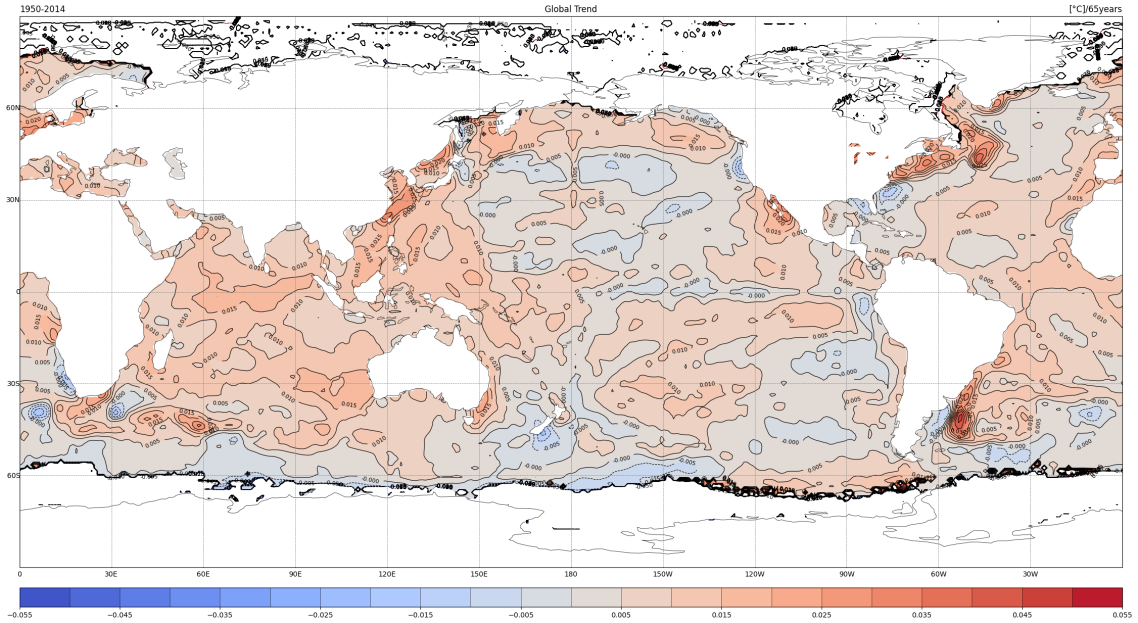

(a)

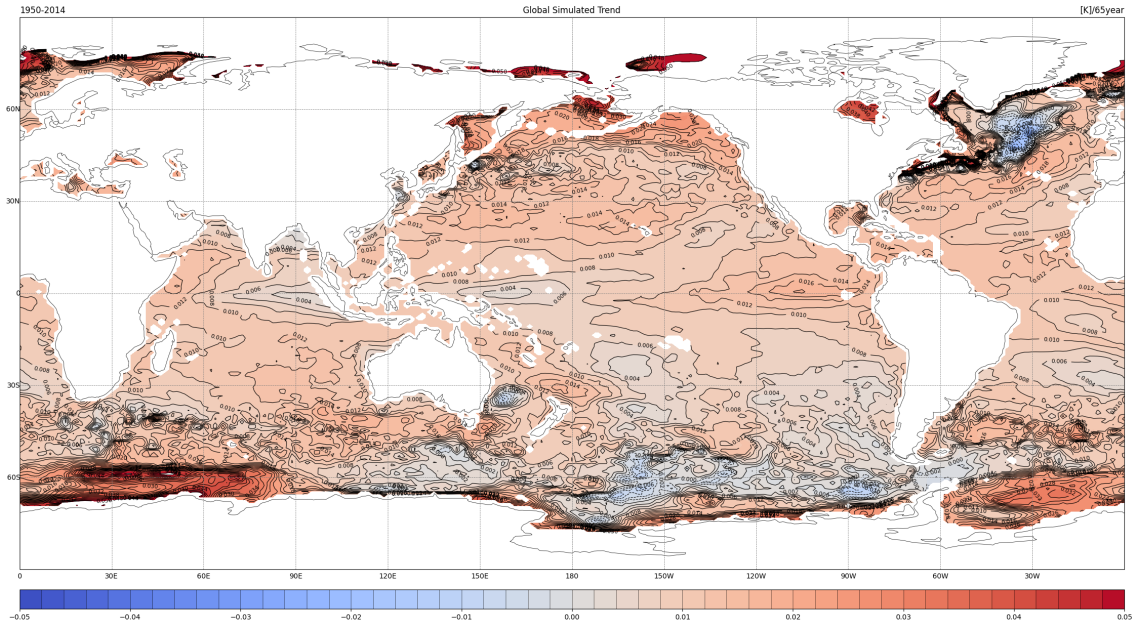

(b)

Figure 4.3: Observed SST trends from the HadISST data set for the period 1950-2014 (1°C/65years) in (a) compared to the simulation of the same period from the CMCC model (1K/65years) in (b).

2. about the northern offshore Pacific, constant or cooling trends have shown in the observational data set, while in the simulation this area undergoes a

warming that is about ∼0.65-0.9K;

3. the SST gradient between coastal Greenland and the northern American west coast is overall well represented, showing slightly more enhanced polarities in the CMCC-CM2 simulation;

4. the spread warming in the Indian Ocean is correctely represented in CMCC-CM2, with increments that are consistent with HadISST (∼0.8K).

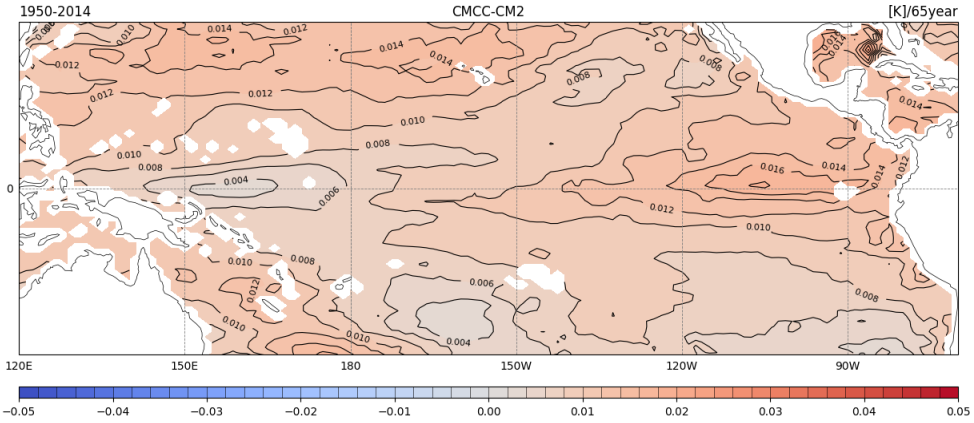

Figure 4.4: The CMCC-CM2 simulated trends over the 1950-2014 period.

It has been said that the exaggerated warming in the cold tongue region is a common bias in climate modelling, that according to Seager et al.[9] is due to a wrong setting in wind speed and humidity that does not correctly take into account the effect of rising GHGs on ocean dynamics. The observed tropical Pacific SST trend is largely reproduced by climate models only adjusting the rising CO_2 and changing wind stress, the latter being enhanced by the strong gradient caused by ocean dynamic response. In this respect it is useful to compare the CMCC-CM2 model (Fig. 4.4) with the CMIP6 and LENS means (Fig. 4.1(b) and (c)).

The CMCC-CM2 trends also misrepresents SST in this area, with a magnitude of warming that is similar to the CMIP6 and LENS multimodel means (∼0.8K). While the latter display homogeneous warming in almost the entire region, the first tend to invert the polarities of the east-west and the north-south gradients. All of these models inaccurately depict the tropical Pacific's reaction to increasing CO_2 due to their cold tongue bias.

The significant impact of the tropical Pacific on global climate suggests that historical and future patterns will differ from those projected by coupled climate models.

Conclusions

Sea Surface Temperatures (SST) are a source of vital information about the climate system and they can provide a powerful instrument to predict its evolution through numerical modelling, hence climatologist need to understand the dynamics that regulate their variability.

In this thesis SSTs have been analyzed, provided by the Met Office Hadley Centre's Sea Ice and Sea Surface Temperature (HadISST) data set, which records the monthly averages of SST from 1870 to 2020. Prior to processing data it was briefly discussed how these can be reconstructed if missing and how they are manipulated to improve calculation time and costs. The basis of Empirical Orthogonal Function analysis has been discussed, in order to understand how a purely theoretical and abstract mathematical model can be used to find patterns of variability in a real complex system. In addition some fundamental of ocean dynamics and climate variability have been explained.

The analysis of Sea Surface Temperatures consisted in representing the HadISST data set as a three dimensional grid (latitude, longitude and time) and computing SST trends. Dividing the time series into 5 periods of thirty years from 1870 to 2020, the linear regression was performed, and it was discovered a general global increase of SSTs.

Although a general global warming, it has been noted that some regions cooled, in contrast with nearby zones of enhanced warming. The cool Greenland coast is opposite to the warm northern American west coast, and the cool eastern equatorial Pacific to a western warm pool. Comparing studies and modeled SSTs, these cooling trends have been connected to the rising of greenhouses gases in the atmosphere, that affects the climate system modifying the way ocean water responds to internal variability events such as upwelling in the Tropical Pacific [9] and the Atlantic Meridional Overturning Circulation (AMOC) [1]. Other regions of interest are the Indian and the northern Pacific Oceans, where a rapid linear warming has been registered in the last 30 years, generating concern about the threatened biodiversity and ecosystems [11]. It has been found that the Indian Ocean is responsible for the major increase of mean global SST the XX century, as its temperature has risen by 1.5°C. It is very likely that this phenomena are due to anthropogenic forcing.

The lack of warming in the cold tongue is a source of information on how the

Pacific Ocean responds to the rising of greenhouse gases, considering that internal variability can only partially explain the phenomenon. It has been found that the vast majority of the climate models generated by the Coupled Model Intercomparison Project Phase 6 (CMIP6) [5] and the Large Ensamble Project (LENS) [6] fail the task of reproducing it, as the simulation means display homogeneous warming over the tropical area, and the phew models that come close to the observation are not statistically relevant. In fact, climate models still fail to reproduce truthfully SST trends because of internal biases due to a non-complete comprehension of how the ocean-atmosphere coupled system is afflicted by the rising concentration of CO_2 that characterize the last 60 years, and that is presumably going to increment in the next decades [9].

Finally, using an historical simulation generated by the Euro-Mediterranean Centre on Climate Change, the CMCC Climate Model Version 2, linear trends have been interpolated for the period 1950-2014. It has been found that this model erroneously depicts a sustained warming over the northern and equatorial Pacific, failing into reproducing the observed trend. Compared to CMIP6 and LENS means, all of them fails into reproducing the north-south and east-west gradients.

As common biases can interfere with prediction, it is crucial for climate scientists to incorporate new data, adjust underlying assumptions, and employ advanced techniques to fill the gap between model simulations and observed SST patterns. Only refining climate modelling it is possible to forecast the future of the global climate system.

Appendix A

Two sided t-test

The hypothesis test is a statistical procedure that allows us to ask a question based on sample information in order to reach a statistically significant decision.

Consider a statistical sample and two hypothesis to evaluate. The *status quo* is the null hypothesis that should be confuted, H_0, while the alternative hypothesis H_a is usually the one that should be proven correct.

As an example, one could try to test whether a calculated trend $\bar{x} = 0$ is a statistical valid mean value or it is rejectable.

Then the hypothesis are the following:

- $H_0 : \mu = \bar{x}$
- $H_a : \mu \neq \bar{x}$

To prove the null hypothesis wrong, the strategy is to find certain statistical properties that the sample does not respect when it should (if H_0 were true). The next step is to choose a significance α level for the distribution. The common standard is $\alpha = 0.05$, that is a level of significance at 95%.

The level of significance of the test indicates the (inverse) probability of incurring in a type I error, that is to reject erroneously the null hypothesis, which was true, accepting the alternative hypothesis, whereas accepting as valid the null hypothesis, when it had to be rejected as false, consist in an error of type II.

In the two-sided hypothesis there will be two critical regions at either end of the curve, each representing a level $\alpha/2$ (Fig. A.1).

For a sufficiently large number of population N, data follows the normal distribution, being shaped as a bell centered around a mean value μ of width σ, where the latter is the standard deviation and it denotes the amplitude within the 68% of the data is contained.

Any normal distribution $G(x)$ can be transformed into a zero-centered normal distribution with unitary standard deviation using the following variable:

$$z = \frac{x - \mu}{\sigma_{\bar{x}}} \tag{A.1}$$

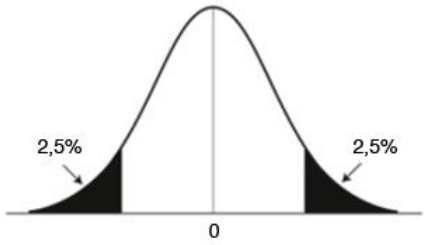

Figure A.1: Normal distribution. The colored areas are the critical regions, where the cumulative probability of finding a mean value is less than 95%.

Where $\sigma_{\bar{x}}$ refers to the standard deviation associated to a sample of mean values $\bar{x}$ and is given by:

$$\sigma_{\bar{x}} = \frac{\sigma}{\sqrt{N}} \tag{A.2}$$

In a normal distribution centered around 0, for a 95% level of accuracy, -1.96 and +1.96 are the critical values, namely there is only a 5% probability of finding $|z| \geq 1.96$. Assuming that H_0 is true, so with $\mu = 0$, a distribution of z that departs substantially from 0 leads to doubting of H_0. There is no way to say with absolute certainty that H_0 is wrong, but for statistical significance, it's conventional to affirm that something that would only happen by chance on 5% of occasions is too rare, and that the available evidence does not support H_0. It is then possible to assume that H_a is true.

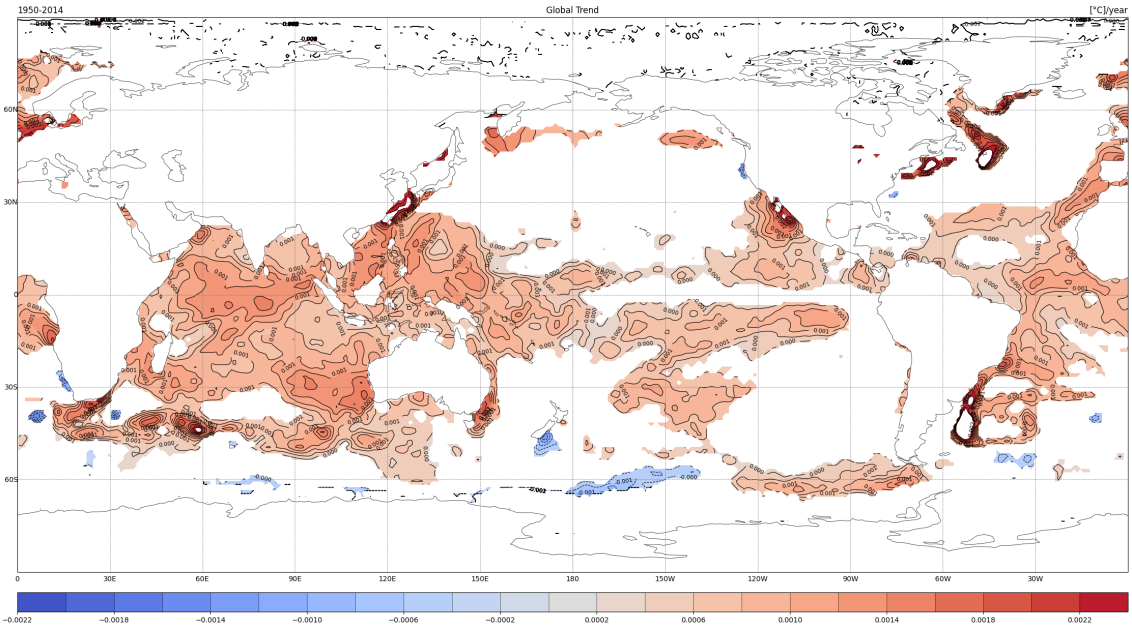

Figure A.2: 95% confidence two-sided t-test performed on the 1958-2018 SST trends (°C/y). All the coordinates that have a probability of finding a null trend superior to 5% have been removed.

Bibliography

[1] Caesar L. et al. "Observed fingerprint of a weakening Atlantic Ocean overturning circulation". In: *Nature* 556 (2018), pp. 191–196. DOI: 10.1038/s41586-018-0006-5.

[2] Cane M. A. et al. "Twentieth-Century Sea Surface Temperature Trends". In: *Science* 275.5302 (1997), pp. 957–960. DOI: 10.1126/science.275.5302.957. URL: http://www.sciencemag.org.

[3] Cherchi A. et al. "Global mean climate and main patterns of variability in the CMCC-CM2 coupled model." In: *Journal of Advances in Modeling Earth Systems* 11.1 (2019), pp. 185–209. DOI: 10.1029/2018MS001369.

[4] Deser C. et al. "Sea Surface Temperature Variability: Patterns and Mechanisms". In: *Annual Reviews* (2010), pp. 115–143. DOI: 10.1146/annurev-marine-120408-151453. URL: marine.annualreviews.org.

[5] Eyring V. et al. "Overview of the Coupled Model Intercomparison Project Phase 6 (CMIP6) experimental design and organization". In: *Geoscientific Model Development* 9 (2016), pp. 1937–1958. DOI: 10.5194/gmd-9-1937-2016. URL: http://www.geosci-model-dev.net/9/1937/2016/.

[6] Kay et al. "The Community Earth System Model (CESM) Large Ensemble Project: A Community Resource for Studying Climate Change in the Presence of Internal Climate Variability". In: *Bulletin of the American Meteorological Society* 96 (2015), pp. 1333–1349. DOI: 10.1175/BAMS-D-13-00255.1. URL: http://www.geosci-model-dev.net/9/1937/2016/.

[7] Rayner N.A. et al. "Global analyses of sea surface temperature, sea ice, and night marine air temperature since the late nineteenth century". In: *Journal of Geophisycal Research* 108.D14 (2003). DOI: 10.1029/2002JD002670. URL: https://marine.annualreviews.org.

[8] Roxy M. K. et al. "The Curious Case of Indian Ocean Warming". In: *Journal of Climate* 27 (2014), pp. 8501–8509. DOI: 10.1175/JCLI-D-14-00471.1.

[9] Seager R. et al. "Strengthening tropical Pacific zonal sea surface temperature gradient consistent with rising greenhouse gases". In: *Nature Climate Change* 9 (2019), pp. 517–522. DOI: 10.1038/s41558-019-0505-x.

[10] Wu Z. et al. “The long-term spatiotemporal variability of sea surface temperature in the northwest Pacific and China offshore”. In: *Ocean Science* 16 (2020), pp. 83–97. DOI: 10.5194/os-16-83-2020.

[11] Xiu P. et al. “Future changes in coastal upwelling ecosystems with global warming: The case of the California Current System”. In: *Scientific Reports* 8.2866 (2018).

[12] Stefanini C. “Caratteristiche della circolazione oceanica e impatto dell’Oceano Atlantico sul clima europeo”. In: (). Available online. URL: http://www.meteonetwork.it/.

[13] Karnauskas K. B. Coats S. “Are Simulated and Observed Twentieth Century Tropical Pacific Sea Surface Temperature Trends Significant Relative to Internal Variability?” In: *Geophysical Research Letters* 44 (2017), pp. 9928–9937. DOI: 10.1002/2017GL074622.

[14] Alexander M. A. Deser C. Phillips A. S. “Twentieth century tropical sea surface temperature trends revisited”. In: *Geophysical Research Letters* 37 (2010). DOI: 10.1029/2010GL043321.

[15] Dodov B. Dijkstra H. “Anatomy of a Climate Model”. In: (2020). Available on line. URL: https://www.air-worldwide.com/publications/air-currents.

[16] Johns W. Kadko D. “Inferring upwelling rates in the equatorial Atlantic using 7Be measurements in the upper ocean”. In: *Deep-Sea Research I* 58 (2011), pp. 647–657. URL: https://arc.fiu.edu/wp-content/uploads/2014/04/Kadko-and-Johns2011.pdf.

[17] Amaya D. J. Karnauskas K. B. Zhang L. “The Atmospheric Response to North Atlantic SST Trends, 1870–2019”. In: *Geophysical Research Letters* 48 (2021). DOI: 10.1029/2020GL090677.

[18] Xie S. P. Kosaka Y. “Recent global-warming hiatus tied to equatorial Pacific surface cooling”. In: *Nature* 501 (2013), pp. 403–407.

[19] MetOffice. “El Niño Southern Oscillation (ENSO) region sea surface temperature forecasts”. In: *https://www.metoffice.gov.uk/* (2023). Available on line.

[20] Marotzke J. Olonscheck D. Rugenstein M. “Broad Consistency Between Observed and Simulated Trends in Sea Surface Temperature Patterns”. In: *Geophysical Research Letters* 47 (2020). DOI: 10.1029/2019GL086773.

[21] Cane M. Seager R. Henderson N. “Persistent Discrepancies between Oserved and Modeled Trends in The Tropical Pacific Ocean”. In: *Journal of Climate* 35 (2022), pp. 4571–4582. DOI: 10.1175/JCLI-D-21-0648.1. URL: https://marine.annualreviews.org.

[22] Latif M. Semenov V. A. “Impact of tropical Pacific variability on the mean North Atlantic thermohaline circulation”. In: *Geophysical Research Letters* 33 (2006), pp. 115–143. DOI: 10.1029/2006GL026237.

[23] Navarra A. Simoncioni V. *A Practical Guide to Empirical Orthogonal Functions*. 2010.

[24] ElDyn G. Wyrtki K. "Equatorial Upwelling Events in the Central Pacific". In: *Journal of Physical Oceanography* 12 (1982), pp. 984–988. URL: `http://www.sciencemag.org`.

[25] Wang F. Yang H. "Notes and Correspondence Revisiting the Thermocline Depth in the Equatorial Pacific". In: *Journal of Climate* 22 (2009), pp. 3856–3863. DOI: `10.1175/2009JCLI2836.1`.